

H-Probe: Estimating Traffic Correlations from Sampling and Active Network Probing

Amr Rizk, Zdravko Bozakov, and Markus Fidler
Institute of Communications Technology, Leibniz Universität Hannover
{amr.rizk, zdravko.bozakov, markus.fidler}@ikt.uni-hannover.de

Abstract—An extensive body of research deals with estimating the correlation and the Hurst parameter of Internet traffic traces. The significance of these statistics is due to their fundamental impact on network performance. The coverage of Internet traffic traces is, however, limited since acquiring such traces is challenging with respect to, e.g., confidentiality, logging speed, and storage capacity. In this work, we investigate how the correlation of Internet traffic can be reliably estimated from random traffic samples. These samples are observed either by passive monitoring within the network, or otherwise by active packet probes at end systems. We analyze random sampling processes with different inter-sample distributions and show how to obtain asymptotically unbiased estimates from these samples. We quantify the inherent limitations that are due to limited observations and explore the influence of various parameters, such as sampling intensity, network utilization, or Hurst parameter on the estimation accuracy. We design an active probing method which enables simple and lightweight traffic sampling without support from the network. We verify our approach in a controlled network environment and present comprehensive Internet measurements. We find that the correlation exhibits properties such as long range dependence as well as periodicities and that it differs significantly across Internet paths and observation times.

I. INTRODUCTION

Traffic characteristics play a key role in planning and operation of packet data networks. As a consequence, in recent years network measurements have attracted considerable attention as a practical method for inferring traffic properties. The scope of such measurements varies from access networks to backbone networks or even across the Internet.

Numerous comprehensive measurement studies, based on recorded network traces, have revealed that aggregate Internet traffic possesses long memory correlations, so-called long range dependence (LRD) [8], [12], [19], [30]. The impact of LRD on network performance was investigated in several works, e.g., [10], [11], [20], [25], [26], [28], [34], [35]. Networks fed with LRD traffic exhibit a fundamentally different behavior compared to systems fed with memoryless or Markovian traffic.

In practice continuous logging and evaluation of all relevant network events in large networks is typically not feasible due to efficiency, confidentiality, and cost factors. For example, with link speeds of 10 Gbps and more capturing traffic traces becomes increasingly difficult, as suitably large and fast storage systems are expensive. One main challenge is therefore, to extract the desired information from a subset of events, e.g., using a sampling procedure that yields consistent estimates of the target metric. In addition, ISPs rarely disclose

traffic traces because of confidentiality issues such that traffic characteristics can only be inferred from external observations. Further, a fundamental limitation of traffic traces is that these reflect traffic characteristics at only a *single* observation point.

In this work, we investigate the problem of estimating the correlation of Internet traffic given a limited set of random samples. First, we consider passive sampling, i.e., capturing traffic samples at some directly accessible node, e.g., a router. Here, the main focus is on the choice of the sampling process and its properties. Further, for any practical realization passive sampling yields a finite sample size, which directly influences the accuracy of the results. Secondly, we consider active probing that is a technique, where external measurements of specific probe packets are used. The aim is to avoid any particular network support by exploiting, e.g., timing information that is imprinted on the probes by interaction with network traffic. The additional challenge of active compared to passive methods is to design probes that actually permit inferring the desired traffic characteristics, which in certain cases may even be impossible [24].

The ultimate result of this work is to enable the online estimation of traffic correlations along network paths without network support. To this end, we present methods for extracting LRD characteristics from sampled traffic. We derive the impact of sampling on the observed traffic correlations for different sampling strategies and show that sampling may distort observations. We develop methods that reverse these effects for a set of sampling processes. We quantify the accuracy of the observations under finite sampling durations, showing that the estimation error increases as τ^{2-2H} with the autocovariance lag τ and the LRD Hurst parameter $H \in (0.5, 1)$. We derive the impact of different sampling parameters on estimation accuracy and show a non-linear trade-off between sampling intensity and sampling duration. Finally, we design and evaluate a practical active probing method to estimate traffic correlations from external observations. We present practical testbed and Internet measurement results showing a complex covariance structure of Internet traffic that exhibits LRD as well as periodic behavior.

The paper is structured as follows: In the next section we present the state-of-the-art on LRD network traffic characteristics, sampling and active network probing. In Sect. III we derive our main results concerning traffic sampling and the accuracy of the estimated traffic parameters. In Sect. V we present and deploy an active probing method that uses

packet probes to infer traffic correlations. Sect. VI concludes the paper.

II. RELATED WORK

In the following, we discuss related work on LRD traffic characteristics, sampling and network probing.

A. LRD traffic characteristics

Comprehensive measurements in the 90s, e.g., [8], [12], [19], [30] revealed that aggregate Internet traffic exhibits LRD and self-similarity phenomena, that can be described by the so-called Hurst parameter H . A self-similar stochastic process possesses the same finite dimensional distributions on different time scales except for a rescaling factor which depends on H . The aggregation of multiple traffic sources offers a possible explanation of these characteristics. It was shown in [40] that aggregating many on-off sources with heavy tailed on and off periods yields self-similar LRD traffic. This notion corresponds to file transfers from heavy tailed file size distributions as observed on storage systems [8], [45]. An experimental validation of the relation between self-similarity and heavy-tailed distributions is carried out in [23] on a large-scale experimental facility.

Given a stationary process $Y(t)$, LRD manifests itself in the slow decay of the autocovariance¹ $c_Y(\tau)$ such that

$$c_Y(\tau) \sim \sigma_Y^2 \tau^{2H-2} \quad \text{for } \tau \rightarrow \infty, \quad (1)$$

where σ_Y^2 is the variance of $Y(0)$ and the Hurst parameter $H \in (0.5, 1)$. The sum of the autocovariance over all lags τ diverges, i.e., $\sum_{\tau} c_Y(\tau) \rightarrow \infty$.

In this work, we focus on the autocovariance structure of (1). Our goal is to infer (1) from traffic observations, respectively, to estimate the Hurst parameter H from the slope of $c_Y(\tau)$ on a log-log scale. Numerous other methods exist for estimating the Hurst parameter from LRD and self-similar time series [4], [39], [42].

In addition to (1), we consider two established methods for estimating the Hurst parameter H [4], [39]. First, we consider the aggregate variance method, that relies on the convergence rate of the sample mean of an LRD process to the true mean. Given samples of $Y(t)$ of size M , the variance of the sample mean decays as $\sim M^{2H-2}$ with growing M .

The second method denoted power spectral density method relies on the behavior of the spectral density of the LRD process $Y(t)$. The spectral density $\Psi_Y(f)$ of $Y(t)$ is well known [4]. It can be approximated as

$$\Psi_Y(f) \sim |f|^{1-2H} \quad \text{for } f \rightarrow 0. \quad (2)$$

The Hurst parameter H can be estimated from the slope of $\Psi_Y(f)$ plotted against the frequency f on a log-log scale.

¹Throughout this work, we use the definition of autocovariance in the signal processing sense, i.e., for a stationary process $Y(t)$ the autocovariance is defined as $c_Y(\tau) := \mathbb{E}[Y(t)Y(t+\tau)] - \mathbb{E}[Y(t)]\mathbb{E}[Y(t+\tau)]$. For brevity, we frequently use the term covariance to mean autocovariance.

B. Sampling

Sampling is widely used to reduce the data processing and storage requirements as well as to circumvent problems, such as system inaccessibility and hardware access latency. A fundamental result often employed in the sampling context is known as PASTA, Poisson Arrivals see Time Averages [46]. PASTA states that the portion of Poisson arrivals that see a system in a certain state corresponds, in average, to the portion of time the system spends in that state.

Further, the authors of [27] establish general conditions, such that Arrivals See Time Averages (ASTA) holds, i.e., bias free estimates are not limited to Poisson sampling. In a recent work the authors of [3] coined the term NIMASTA, i.e. Non-intrusive Mixing Arrivals See Time Averages, in the context of network measurements. Using an argument on joint ergodicity, the authors prove an almost sure convergence of

$$\lim_{N \rightarrow \infty} \frac{1}{N} \sum_{i=1}^N g(Y(\theta_i)) = \mathbb{E}[g(Y(0))] \quad (3)$$

where $Y(\theta_i)$ is a sample of the process $Y(t)$ at time θ_i and g is a general positive function of Y . The sampling times θ_i for $i \in \mathbb{N}$ are chosen according to a sampling process. The target metric is specified depending on the chosen function g . Eq. (3) is satisfied when the process $Y(t)$ is ergodic and the sampling process is mixing [3]. The authors in [2] show that Poisson sampling, though bias free, does not guarantee minimum variance estimates.

A comparison of Poisson and periodic sampling was carried out in [37], [41]. In [41] the authors show experimentally, that the differences between round trip times (RTT), loss rate and packet pair dispersion estimates, obtained by either Poisson or periodic probing, are in some cases not significant. Depending on the autocovariance of the sampled process, Poisson or periodic sampling can be superior. This is shown in [37] using the metric asymptotic variance.

In [31] it is shown that for correlation lags tending to infinity, random sampling captures the long memory of the original processes, as long as the sampling distribution has a finite mean.

C. Active network probing

The injection of test packets into a network for inferring network performance, i.e., active probing, has attracted considerable attention in recent years. End-to-end packet delays or inter packet times are metrics commonly used to estimate network characteristics such as the average available bandwidth or even to reconstruct statistics of the cross-traffic [17], [18], [33], [38]. Under the assumption of FIFO scheduling, cross traffic intensity can be estimated from the dispersion of back-to-back probing packets [9], [21], [22], [38].

Cross traffic estimation of LRD traffic using active measurements was discussed, in [16], [32]. The authors of [16] carry out a numerical simulation to interpolate cross traffic from probes and predict future traffic from the LRD property. In [32] the authors derive and show simulation results for a

deterministic probing scheme based on a multi-fractal wavelet traffic model. Essential to their estimation is the assumption that the queue does not empty between the the individual packets of a packet probe. Our work differs from [16], [32] as we examine different *random* sampling distributions and show how to extract traffic correlations from distorted observations.

Two important aspects concerning network probing are the measurement intrusiveness and the interaction of probes with the measured system. The first aspect is usually addressed by minimizing the probing rate while controlling the quality of the results. The second aspect is more involved, since the probes perturb the system leading to distorted observations. For example, measuring queueing delays of probes to determine the true queue length distribution is governed by a type of Heisenberg uncertainty [36], since the probes alter the queue length. The authors describe the impact of the probing intensity on the accuracy of the result using the notion of asymptotic variance. The effect is increased in case of LRD traffic, although not given in closed form, leading to higher uncertainty in the estimated waiting time [36].

III. TRAFFIC SAMPLING AND PARAMETER ESTIMATION

In this section we derive our main results on traffic covariance estimation from sampled observations. Based on sampling properties we present rigorous traffic parameter estimation. Subsequently, we investigate the accuracy of the estimates under the practical constraint of finite sample sizes.

A. Covariance of sampled processes

We define a sampling model comprising of three stationary discrete time processes: a traffic increment process $Y(t)$, a sampling process $A(t)$, and an observed process $W(t)$ for $t \in \mathbb{N}_0$. We assume statistical independence of $A(t)$ and $Y(t)$. Our focus lies on the estimation of the covariance of $Y(t)$ that is characterized by LRD. While the LRD process may be in continuous time, we regard its increments on a fixed time slot basis, and hence the discretization of $Y(t)$.

The sampling process $A(t)$ is a point process taking the value of one whenever a sample is taken, and zero otherwise, i.e., $A(t)$ is a Kronecker delta train, where a Kronecker delta is defined as $\delta(n) = 1$ for $n = 0$ and zero otherwise. The process has independent and identically distributed (iid) inter-sample times drawn from a given probability distribution F . The inter-sample time is the time between two consecutive Kronecker deltas. The sampling intensity, i.e., the mean rate of the sampling process of $A(t)$, is $E[A(t)] = \mu_A$ for all t , with $0 \leq \mu_A \leq 1$. Throughout this work we use $\mu_{(\cdot)}$ to denote the expected value $E[(\cdot)]$.

We base our analysis on the observed stochastic process $W(t)$, generated by random samples $A(t)$ of the increment process $Y(t)$, with

$$W(t) = A(t)Y(t). \quad (4)$$

We aim to infer properties of the traffic process $Y(t)$ from the observation process $W(t)$. In particular, we are interested

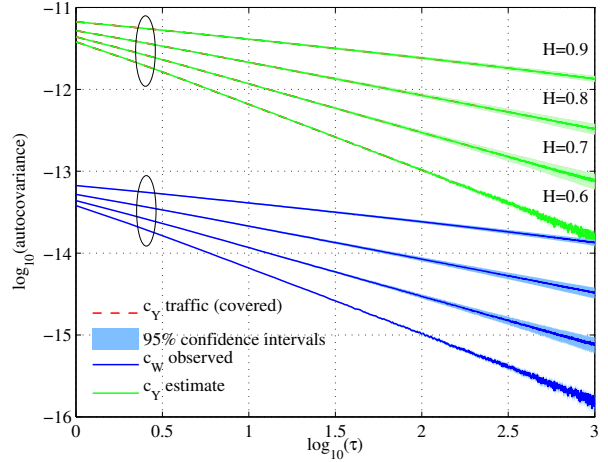


Fig. 1: Autocovariance of LRD traffic processes under geometric sampling. The observed “ $c_W(\tau)$ ” maintains the autocovariance structure of the traffic process. The covariance of the original process “ $c_Y(\tau)$ (traffic)” is exactly covered by the reconstructed “ $c_Y(\tau)$ (estimate)”.

in sampling distributions F that deliver accurate estimates of the correlations of the LRD traffic process $Y(t)$ and the associated Hurst parameter H . Extracting the autocovariance of the process $Y(t)$, i.e., $c_Y(\tau)$ from the observed $c_W(\tau)$ is generally not a straightforward task. The following lemma reveals the impact of sampling on the autocovariance of the observed process. The proof of Lem. 1 is a variation of standard technique in stochastics.

Lemma 1: Given the stationary and independent stochastic processes $A(t)$ and $Y(t)$ and let $W(t) = A(t)Y(t)$. The covariance of $W(t)$ can be decomposed into

$$c_W(\tau) = (c_A(\tau) + \mu_A^2) c_Y(\tau) + c_A(\tau) \mu_Y^2.$$

Proof: Given independent and stationary processes $A(t)$ and $Y(t)$. Let $W(t) = A(t)Y(t)$. It follows that

$$\begin{aligned} c_W(\tau) &= E[A(t)A(t+\tau)] E[Y(t)Y(t+\tau)] - \mu_A^2 \mu_Y^2 \\ &= (c_A(\tau) + \mu_A^2) (c_Y(\tau) + \mu_Y^2) - \mu_A^2 \mu_Y^2 \\ &= (c_A(\tau) + \mu_A^2) c_Y(\tau) + c_A(\tau) \mu_Y^2 \end{aligned}$$

where $c_{(\cdot)}(\tau)$ denotes the covariance of process (\cdot) at lag τ . ■

Lem. 1 clearly shows the impact of the sampling process on the observed covariance. In particular, the choice of the inter-sample distribution influences $c_W(\tau)$ through μ_A and $c_A(\tau)$, i.e., both the sampling intensity and the sampling covariance influence the observation.

In this work, we investigate four inter-sample distributions: geometric (memoryless), periodic, Gamma, and uniform. For each distribution we show how to recover the covariance of the LRD process $c_Y(\tau)$ from the observed $c_W(\tau)$ using the covariance $c_A(\tau)$. To this end, we derive the covariance of the sampling process $c_A(\tau) = E[A(t)A(t+\tau)] - \mu_A^2$. We use the

TABLE I: Parametrization of sampling distributions and traffic parameter estimation

	inter-sample distribution $f(\tau)$	autocovariance $c_A(\tau) =$ $E[A(t)A(t+\tau)] - \mu_A^2$ for $\tau > 0$	reconstructed traffic autocovariance $c_Y(\tau)$	remarks
Geometric	$p(1-p)^{\tau-1}$	0	$\frac{c_W(\tau)}{\mu_A^2}$	$\mu_A = p$
Periodic	$\delta(\tau - \Delta)$	$1/\Delta - 1/\Delta^2$ for $\tau = k\Delta, k \in \mathbb{N}$ $-1/\Delta^2$ otherwise	$\frac{c_W(\tau) - \mu_A \mu_Y^2 (1 - \mu_A)}{\mu_A}$	$c_Y(\tau)$ at $\tau = k\Delta,$ $\mu_A = 1/\Delta$
Gamma	$\frac{\beta^\alpha}{\Gamma(\alpha)} \tau^{\alpha-1} e^{-\beta\tau}$	$-\mu_A^2 e^{-4\mu_A\tau}$	$\frac{c_W(\tau) + \mu_A^2 \mu_Y^2 e^{-4\mu_A\tau}}{\mu_A^2 (1 - e^{-4\mu_A\tau})}$	for $\alpha = 2, \mu_A = \frac{\beta}{\alpha}$
Uniform	$1/b$ for $0 \leq \tau \leq b$	$\mu_A^2 \left(\frac{1}{2} e^{\frac{1}{2}\mu_A\tau} - 1 \right)$	$\frac{c_W(\tau) - \mu_A^2 \mu_Y^2 \left(\frac{1}{2} e^{\frac{1}{2}\mu_A\tau} - 1 \right)}{\mu_A^2 \frac{1}{2} e^{\frac{1}{2}\mu_A\tau}}$	$c_Y(\tau)$ for $\tau \leq b,$ $\mu_A = 2/b$

probability mass function $f(\tau)$ of the inter sample times to calculate the n -fold self-convolution $f^{(*n)}(\tau)$. We then calculate the autocorrelation $E[A(t)A(t+\tau)] = \mu_A \sum_{n=1}^{\infty} f^{(*n)}(\tau)$ as given in [7], Eq. (4.6.1). We exploit the property that $f^{(*n)}$ is a power series for the considered distributions and that its sum converges. The derivation of the autocorrelations used in Tab. I is given in appendix VII-A to VII-D. In the last step we insert $c_A(\tau)$ into Lem. 1 and solve for $c_Y(\tau)$.

Tab. I summarizes the expressions used to reconstruct $c_Y(\tau)$ given specific inter-sample distribution parameters and corresponding $c_A(\tau)$. First, we consider the geometric inter-sample distribution, i.e., a Bernoulli sampling process. The independence of the increments implies that $c_A(\tau) = 0$ for $\tau > 0$. From Lem. 1, the observations $W(t)$ have autocovariance

$$c_W(\tau) = c_Y(\tau)\mu_A^2. \quad (5)$$

This shows that sampling processes with uncorrelated increments only shift the autocovariance structure of the sampled process $Y(t)$ by μ_A^2 .

Next, we consider periodic sampling, where $A(t)$ is modeled as a comb of Kronecker deltas with sampling period Δ . The mean intensity of the sampling process is $\mu_A = 1/\Delta$. We can recover $c_Y(\tau)$ using Lem. 1, however, only at $\tau = k\Delta$ where $k \in \mathbb{N}$. To perform this inference, the mean rate μ_Y of the traffic process $Y(t)$ must be known. Due to the rigid structure of periodic sampling it is, however, shown that the

mean rate estimator μ_W/μ_A is not unbiased [3], e.g., the sampling period may coincide with periodicities in the original process.

Finally, Tab. I provides expressions for reconstructing $c_Y(\tau)$ after Gamma and uniform sampling. For mathematical tractability, here we use continuous time for the derivation of the autocorrelation of $A(t)$. For discretization we use a time slot of unit size. Note that the discretization error diminishes for autocorrelation lags much larger than the discretization time slot. In case of Gamma sampling, the ability to estimate $c_Y(\tau)$ is not limited to the exemplary $\alpha = 2$ given in Tab. I. Lem. 1 can be used to estimate $c_Y(\tau)$ for Gamma sampling processes with arbitrary parameters as long as the autocovariance $c_A(\tau)$ is computable. We provide results for Gamma sampling with $\alpha = 4$ in appendix VII-C. For uniform sampling with support b Tab. I gives a result for lags $\tau \leq b$. Due to the finite support, $c_A(\tau)$ quickly approaches zero for $\tau > b$. Like in case of periodic sampling, the reconstruction of $c_Y(\tau)$ from Gamma and uniform sampling, respectively, requires knowledge of μ_Y .

Figures 1 and 2 illustrate autocovariance estimates derived from observations $W(t)$, that are obtained by sampling LRD traffic with autocovariance $c_Y(\tau) \sim \sigma_Y^2 \tau^{2H-2}$ and $H \in [0.6, 0.9]$.² We use geometric, periodic, Gamma, and

²Synthetic traces of length 2.5×10^8 time slots were used for the simulation which was repeated 25 times for each considered H .

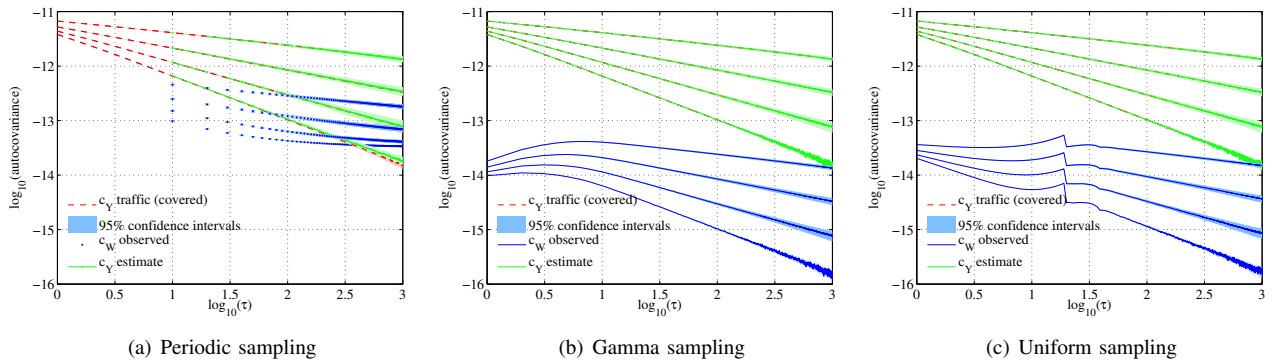


Fig. 2: Autocovariance of the LRD process under different sampling strategies. Note that “ $c_Y(\tau)$ (traffic)” is covered by the “ $c_Y(\tau)$ (estimate)”.

uniform inter-sample time distributions and set $\mu_A = 0.1$. In all cases the reconstructed autocovariance denoted “ $c_Y(\text{estimate})$ ” exactly covers the original traffic autocovariance “ $c_Y(\text{traffic})$ ”.

Geometric sampling in Fig. 1 preserves the linear covariance structure of $c_Y(\tau)$. The observed $c_W(\tau)$ is vertically shifted by $\log(\mu_A^2)$ w.r.t. the original $c_Y(\tau)$. The Hurst parameter H can be inferred directly from the slope of $c_W(\tau)$.

For the remaining distributions shown in Fig. 2, the observations $c_W(\tau)$ are distorted. However, using Lem. 1 we recover the original covariance $c_Y(\tau)$. Using the expressions from Tab. I we reconstruct “ $c_Y(\text{estimate})$ ” which lies on top of the original autocovariance “ $c_Y(\text{traffic})$ ”.

In the following we discuss advantages and disadvantages of the presented sampling distributions. Periodic and uniform sampling are practically convenient as the inter-sample times cannot become arbitrarily large due to the finite support of the inter-sample distribution. Moreover, periodic sampling is easy to implement.

However, it is important to point out that periodic sampling yields misleading results if the sampling period coincides with periodicities in the target process. In addition, periodic, Gamma as well as uniform sampling require a reconstruction step to estimate the covariance $c_Y(\tau)$ from observations as shown above. To this end, an estimate of μ_Y is required.

Memoryless sampling is proposed by the IETF as a network probing scheme [29]. We find that a major advantage of geometric sampling, i.e., memoryless, is that the covariance structure of $c_Y(\tau)$ is preserved in the observations as given in (5). This stands in contrast to periodic, Gamma and uniform sampling. In the following we continue the analysis with geometric sampling because of its advantages discussed above.

B. Impact of finite sample sizes

Next, we examine the accuracy of the derived estimates for finite sample sizes as this is important for any practical realization. We determine the impact of sampling parameters, e.g., sampling duration or intensity, on the observations. Moreover, we evaluate the accuracy of the deployed statistical estimators. Finally, we recover the results from Sect. III-A in the limit for infinite sampling durations.

We investigate sample autocovariances marked by $\tilde{c}_{(\cdot)}$ as estimators of the population autocovariances $c_{(\cdot)}$. In addition, we consider the sample means $\tilde{\mu}_{(\cdot)}$ as estimators of the population means $\mu_{(\cdot)}$. To better understand the impact of finite sample sizes on the observations and the covariance estimates we examine the individual effects of the sample covariances involved in a step by step manner.

While geometric sampling is appealing since it's autocovariance $c_A(\tau) = 0$ for $\tau > 0$, it loses this property for finite sampling duration T , where T is the length of the time-slotted sampling process $A(t)$ in slots.

In the following we focus on three aspects. First in subsection III-B1, we derive the impact of finite sample sizes on the observability of the covariance of sampled traffic. The second aspect is the impact of the sample covariance $\tilde{c}_A(\tau)$ and its influence on the estimation error. This is handled in subsection

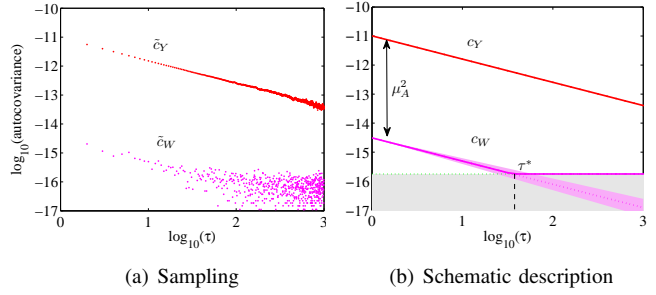


Fig. 3: Noisy observations due to finite sampling. Noise floor (shaded area) in Sect. III-B1. Noise cone in Sect. III-B2.

III-B2. The third aspect is the impact of finite sample sizes on the bias of the covariance estimators given in subsection III-B3.

1) Observation limit: In this section, we consider observations from finite sampling. At first, we do not consider deviations of sample statistics from respective population measures. This assumption is relaxed in the following subsections. We investigate the limit up to which the covariance of the observed LRD process $\tilde{c}_W(\tau)$ can be distinguished from the covariance of iid sequences of the same sample size. Obeying this limit ensures that the variability that is due to the sample size does not mask the covariance that we seek to observe. Exemplary, we depict in Fig. 3(a) the sample autocovariance $\tilde{c}_Y(\tau)$ of an LRD traffic trace $Y(t)$, and the corresponding autocovariance of geometrically sampled observations $\tilde{c}_W(\tau)$, both with a limited sample size T . Evidently, $\tilde{c}_W(\tau)$ is not just a shifted version of $\tilde{c}_Y(\tau)$ but distorted for increasing lags τ by observation “noise” that stems from the variability of the limited sample size.

We seek a range of lags $\tau \in [0, \tau^*]$ in which the covariance of the sampled process can be observed without significant distortion. Based on a standard technique [4] we compare the covariance of the observed process to the covariance of geometrically sampled iid Gaussian sequences to obtain τ^* up to which both covariances are significantly different.

We define τ^* as the intersection of $c_W(\tau)$ from (5) and the 0.95 confidence interval for geometrically sampled finite Gaussian iid sequences with mean μ_Y and variance σ_Y^2 . For $T \gg \tau$ we find that this confidence interval is given by $2\sqrt{(\sigma_A^2\mu_Y^2 + \mu_A\sigma_Y^2)^2 + 4\mu_A^2\mu_Y^2(\sigma_A^2\mu_Y^2 + \mu_A\sigma_Y^2)}/\sqrt{T}$. The calculation relies on the central limit theorem and is given in detail in appendix VII-E. Fig. 3(b) depicts τ^* as well as the confidence interval, denoted as noise floor, schematically.

To calculate τ^* for LRD traffic with covariance $c_Y(\tau) = K\sigma_Y^2\tau^{2H-2}$, with constant K , we equate the above confidence interval with $c_W(\tau) = c_Y(\tau)\mu_A^2$ from (5) to obtain

$$\tau^* = \left[\frac{K\sigma_Y^2\mu_A^2\sqrt{T}}{2\sqrt{(\sigma_A^2\mu_Y^2 + \mu_A\sigma_Y^2)^2 + 4\mu_A^2\mu_Y^2(\sigma_A^2\mu_Y^2 + \mu_A\sigma_Y^2)}} \right]^{\frac{1}{2-2H}}.$$

It is obvious that stronger LRD, i.e., higher H , is observed

better. Clearly, for an infinite sample size $T \rightarrow \infty$, the observable range goes to infinity $\tau^* \rightarrow \infty$. Fig. 3(a) shows that in practice it is important to consider this range to ensure that the results are not strongly distorted.

2) **Estimation accuracy:** Next, we evaluate the impact of the finite sample size on the sample covariance $\tilde{c}_A(\tau)$. We analyze the influence of $\tilde{c}_A(\tau)$ on the observation $\tilde{c}_W(\tau)$ and of estimates of $c_Y(\tau)$ obtained thereof. For ease of exposition, we assume $\tilde{c}_Y(\tau) = c_Y(\tau)$, $\tilde{\mu}_A = \mu_A$ and $\tilde{\mu}_Y = \mu_Y$, i.e., in this subsection we restrict our analysis to the deviation of $\tilde{c}_A(\tau)$ from $c_A(\tau)$.

We assume $T \gg \tau$ and use the central limit theorem to approximate the distribution of the sample autocovariance $\tilde{c}_A(\tau)$ by a Gaussian distribution with standard deviation $\sigma_A \sqrt{\sigma_A^2 + 4\mu_A^2} / \sqrt{T - \tau}$. From the Bernoulli sampling process $A(t)$ we know that $\sigma_A^2 = \mu_A - \mu_A^2$. We calculate the 0.95 confidence interval $c_A^{.95} \approx \pm 2\sigma_A \sqrt{\sigma_A^2 + 4\mu_A^2} / \sqrt{T - \tau}$ for the mean sample autocovariance³. The derivation can be found in appendix VII-F.

With help of $c_A^{.95}$ we investigate the impact of the variations of $\tilde{c}_A(\tau)$ on the observation $\tilde{c}_W(\tau)$. First, we use $c_A^{.95}$ to calculate a confidence interval for $\tilde{c}_W(\tau)$ from Lem. 1 as $c_W^{.95}(\tau) = \pm c_A^{.95} (c_Y(\tau) + \mu_Y^2)$. We schematically depict $c_W^{.95}(\tau)$ as noise cone in Fig. 3(b).

Next, in reference to (5) we consider the estimator $\tilde{c}_W(\tau) / \mu_A^2$ for estimating $c_Y(\tau)$. We analyze the impact of the variations of $\tilde{c}_A(\tau)$ on this estimator. We calculate the confidence interval $c_Y^{.95}(\tau)$ for this estimator as $c_Y^{.95}(\tau) = \pm c_A^{.95} (c_Y(\tau) + \mu_Y^2) / \mu_A^2$. Finally, we obtain the following relative error

$$\varepsilon_Y^{rel}(\tau) = \frac{|c_Y^{.95}(\tau)|}{c_Y(\tau)} \approx \frac{2\sigma_A \sqrt{\sigma_A^2 + 4\mu_A^2}}{\sqrt{T - \tau} \mu_A^2} \left(1 + \frac{\mu_Y^2}{c_Y(\tau)} \right). \quad (6)$$

From (6) we observe that the estimation error introduced through $\tilde{c}_A(\tau)$ decays with increasing sampling duration T or with increasing sampling intensity μ_A . For small (practical) sampling intensities, e.g., $\mu_A \leq 0.1$, we find a nonlinear trade-off between sample intensity μ_A and sampling duration T . Using $\sigma_A^2 = \mu_A - \mu_A^2$ from the Bernoulli sampling process the prefactor in (6) can be approximated as $1/\sqrt{T}\mu_A$ for $T \gg \tau$. This result enables the important conclusion that for finite sample sizes sampling intensity has a stronger impact on accuracy than sampling duration.

Next, we examine the influence of the parameter H on (6) for large lags τ . For increasing τ , $c_Y(\tau)$ decreases, such that when $c_Y(\tau) \ll \mu_Y^2$, the relative estimation error (6) becomes

$$\begin{aligned} \varepsilon_Y^{rel}(\tau) &\approx \frac{2\sigma_A \sqrt{\sigma_A^2 + 4\mu_A^2}}{\sqrt{T - \tau} \mu_A^2} \left(\frac{\mu_Y^2}{c_Y(\tau)} \right) \\ &\approx \frac{2\sigma_A \sqrt{\sigma_A^2 + 4\mu_A^2} \mu_Y^2}{\sqrt{T - \tau} \mu_A^2 \sigma_Y^2} \tau^{2-2H}, \end{aligned} \quad (7)$$

where we substituted $c_Y(\tau) = \sigma_Y^2 \tau^{2H-2}$. The relative estimation error $\varepsilon_Y^{rel}(\tau)$ increases with the lag τ depending on

³We use the relation \approx to denote the approximation, here due to the central limit theorem.

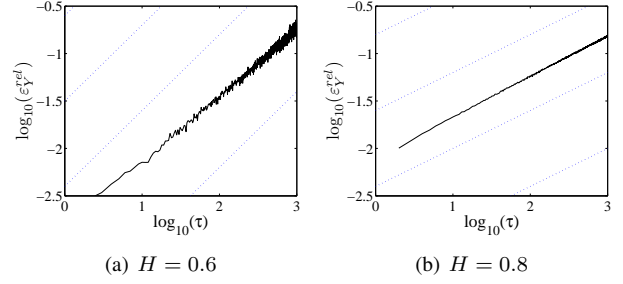


Fig. 4: Estimation error under finite sampling depends on H .

$H \in (0.5, 1)$. For LRD traffic which exhibits large H , the estimation error increases slower in τ compared to traffic with a small parameter H .

We depict $\varepsilon_Y^{rel}(\tau)$ in Fig. 4. To this end, we used 100 generated LRD traffic traces with $T = 2 \times 10^8$ time slots. The figure includes auxiliary lines with a slope of $2 - 2H$. It is evident, that the estimation error evolves with τ as given by (7).

In addition, we calculate the needed sampling duration T to achieve constant ε_Y^{rel} for a given lag τ , and fixed μ_A, μ_Y and σ_Y . We find from (7) that the sampling duration has to increase as $T \sim \max\{\tau^{4-4H}, \tau\}$, which again reveals the impact of H . Specifically, for $H < 0.75$ the sampling duration has to increase faster than linearly with τ to achieve constant ε_Y^{rel} .

3) **Bias of autocovariance estimators:** Next we investigate the accuracy of the deployed statistical estimators. The impact of the finite sample size carries forward to the computation of the autocovariance of $Y(t)$. First we consider the case where we directly observe $Y(t)$ for a finite duration T . We consider the autocovariance estimator $\tilde{c}_Y(\tau) = \frac{1}{T-\tau} \sum_{t=1}^{T-\tau} (y(t) - \tilde{\mu}_{Y_0})(y(t+\tau) - \tilde{\mu}_{Y_\tau})$ with $\tilde{\mu}_{Y_i} = \frac{1}{(T-\tau)} \sum_{t=1}^{T-\tau} y(t+i)$. An estimator of the autocovariance is unbiased iff $E[\tilde{c}_Y(\tau)] = c_Y(\tau)$. To inspect the bias of $\tilde{c}_Y(t)$, we calculate its expected value and find

$$E[\tilde{c}_Y(\tau)] \approx c_Y(\tau) - \frac{\sigma_Y^2}{(T - \tau)^{2-2H}}. \quad (8)$$

The derivation of (8) is given in appendix VII-G.

From (8) we conclude that the autocovariance estimator $\tilde{c}_Y(\tau)$ is asymptotically unbiased for $T \rightarrow \infty$ and $T \gg \tau$. The maximum lag, up to which the autocovariance is estimated, must be chosen carefully, such that the bias in (8) becomes negligible. However, the bias depends on H such that higher H require larger T .

After considering the entire process $Y(t)$ we now investigate the bias of the autocovariance estimator when applied to $W(t)$ as observed by sampling with finite duration T . We calculate the expected value of the estimated autocovariance

$$\begin{aligned} E[\tilde{c}_W(\tau)] &\approx c_W(\tau) - \frac{c_W(0)}{T - \tau} \\ &\quad - \frac{2}{(T - \tau)^2} \sum_{t=1}^{T-\tau-1} (T - \tau - t) c_W(t). \end{aligned} \quad (9)$$

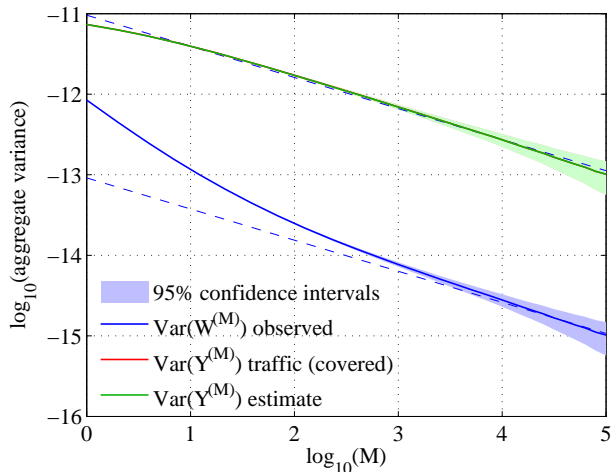


Fig. 5: Aggregate variance estimate under geometric sampling. The variance $\text{Var}(Y^{(M)})$ of the traffic process $Y(t)$ is covered by the estimate obtained from (11) using the variance of the observations $\text{Var}(W^{(M)})$ respectively the sampling process $\text{Var}(A^{(M)})$.

The derivation of (9) is given in appendix VII-H. The bias in (9) goes to zero for $T \rightarrow \infty$ and $T \gg \tau$.

In the remainder of this section we provide brief conclusions that highlight our main findings. We presented a framework for extracting the traffic autocovariance from observed samples. From our evaluation of the sampling distributions we conclude, that the covariance observed under geometric sampling does not exhibit any distortions. This property greatly simplifies the reconstruction of the covariance of the original process $Y(t)$, as no additional parameters, such as μ_Y , must be estimated. Hence, for geometric sampling with sufficiently large T we use $\tilde{c}_W(\tau)/\mu_A^2$ as an estimator of the traffic autocovariance. From the evaluation of the estimator we find two major aspects that limit the observability for finite sampling sizes. First, finite sampling sizes yield computable distortions given in Sect. III-B1 and III-B2 which may obscure the true covariance structure. Secondly, the bias for covariance estimators depends on the Hurst parameter, such that longer measurements must be conducted for traffic exhibiting strong LRD.

Nevertheless, finite sampling effects disappear in the limit for large sampling durations. Moreover, we found that increasing the probing intensity improves estimation results more quickly than increasing the sampling duration.

IV. IMPACT OF SAMPLING ON SELECTED H ESTIMATORS

In this section we analyze the impact of sampling on two established Hurst parameter estimation techniques, i.e., the aggregate variance, respectively, the spectral density method.

A. Aggregate variance

Briefly, the method exploits the fact that the variance of an LRD, self-similar process considered at different aggregation time scales decays linearly in H on a log-log scale. As outlined

in [39], we divide an LRD process $Y(t)$ into blocks of size M , denoted aggregation level, and average within each block. The aggregate time series on the aggregation level M of $Y(t)$ is obtained as

$$Y^{(M)}(k) = \frac{1}{M} \sum_{t=1+(k-1)M}^{kM} Y(t) \quad \text{for } k \in \mathbb{N}. \quad (10)$$

The variance of the sample means is known to decay with the block size as M^{2H-2} . The Hurst parameter H is obtained from the corresponding slope on a log-log scale.

The following lemma shows the impact of the sampling process on the aggregate variance of the observed process $W(t)$.

Lemma 2: Given (4) and the aggregation rule (10). For the aggregate processes $A^{(M)}$, $W^{(M)}$, and $Y^{(M)}$ it holds that

$$\begin{aligned} \text{Var}(W^{(M)}) &= \mu_Y^2 \text{Var}(A^{(M)}) + \mu_A^2 \text{Var}(Y^{(M)}) \\ &+ \frac{1}{M} \sigma_Y^2 \sigma_A^2 + \frac{2}{M^2} \sum_{\tau=1}^{M-1} (M-\tau) c_Y(\tau) c_A(\tau). \end{aligned}$$

The proof of Lem. 2 is given in the appendix VII-I. Lem. 2 illustrates the relation between the variances of the three aggregate processes $A^{(M)}$, $W^{(M)}$ and $Y^{(M)}$. From Lem. 2 we see the impact of sampling on the observed $\text{Var}(W^{(M)})$ through $c_A(\tau)$ and the parameters of $A(t)$, i.e., μ_A and σ_A^2 .

Again the advantage of geometric sampling is apparent as $c_A(\tau) = 0$ allows solving for $\text{Var}(Y^{(M)})$ directly using the variances of the sampling process $\text{Var}(A^{(M)})$, respectively, of the observed process $\text{Var}(W^{(M)})$ as

$$\begin{aligned} \text{Var}(Y^{(M)}) &= \frac{1}{\mu_A^2} \text{Var}(W^{(M)}) \\ &- \frac{1}{\mu_A^2} \left(\mu_Y^2 \text{Var}(A^{(M)}) + \frac{1}{M} \sigma_Y^2 \sigma_A^2 \right). \quad (11) \end{aligned}$$

The estimate $\text{Var}(Y^{(M)})$ in (11) requires estimates of the mean and variance of the traffic process. These estimates can be obtained from $W(t) = A(t)Y(t)$ as $\mu_Y = \mu_W/\mu_A$ respectively $\sigma_Y^2 = (\sigma_W^2 - \sigma_A^2 \mu_Y^2)/\mu_A$ where we used that $\sigma_A^2 + \mu_A^2 = \mu_A$ for the Bernoulli sampling process $A(t)$.

Fig. 5 depicts the decay of $\text{Var}(W^{(M)})$ as a function of M for geometrically sampled observations. We consider the same scenario and parameters as for Fig. 1 in Sect. III-A. Note that $\text{Var}(Y^{(M)})$ of the original process is covered by the estimated aggregate variance using (11), denoted “ $\text{Var}(Y^{(M)})$ estimate”. A Hurst parameter estimate is deduced from the slope of “ $\text{Var}(Y^{(M)})$ estimate”, i.e., $2H - 2$. The correct slope for the evaluated $H = 0.8$ is indicated in the figure by the dashed auxiliary lines.

For the remaining sampling distributions discussed in Sect. III-A the inversion of Lem. 2 for $\text{Var}(Y^{(M)})$ is not easily possible as $c_A(\tau) \neq 0$ such that the term that contains $c_Y(\tau)$ persists.

In general, as the block size M increases, the impact of the terms in the second line in Lem. 2 diminishes, however. For $M \rightarrow \infty$ the relationship in Lem. 2 tends to

$$\text{Var}(W^{(M)}) \approx \mu_Y^2 \text{Var}(A^{(M)}) + \mu_A^2 \text{Var}(Y^{(M)}).$$

In particular, for $M \rightarrow \infty$ the observed $\text{Var}(W^{(M)})$ tends to $\mu_A^2 \text{Var}(Y^{(M)})$. This is due to the fact that sampling processes $A(t)$ considered here are *not* LRD. Hence, $\text{Var}(A^{(M)})$ decays with slope -1 with M on a log-log scale, whereas $\text{Var}(Y^{(M)})$ decays with $2H - 2$. This effect is visible in Fig. 5 as $\text{Var}(W^{(M)})$ tends for increasing M to the auxiliary dashed line of slope $2H - 2$.

B. Spectral density

Spectrum based Hurst parameter estimators rely on the characteristics of the frequency domain representation of LRD processes. The spectral density of an LRD process $Y(t)$ possesses the behavior given in (2) [4], [39]. Hence, H can be estimated from the logarithm of the spectral density of $Y(t)$ plotted vs. $\log(f)$.

We rephrase Lem. 1 for the spectral density to find

$$\Psi_W(f) = \Psi_A(f) * \Psi_Y(f) \quad (12)$$

with $\Psi_{(\cdot)}(f)$ denoting the spectral density of the process (\cdot) . We use $*$ to denote the convolution defined as $x * y(t) := \int_{-\infty}^{\infty} x(\tau)y(t - \tau)d\tau$. To prove (12) we use the Wiener-Khinchin theorem, which states that the spectral density is given by the Fourier transform of the autocorrelation function. The autocorrelation of $W(t) = A(t)Y(t)$, i.e., $E[W(t)W(t + \tau)]$, is obtained as the product of the autocorrelation functions of $A(t)$ and $Y(t)$. Finally, the Fourier transform of the product of two functions $\mathcal{F}\{x \cdot y\}(f)$ is given by the convolution of the respective Fourier transforms $\mathcal{F}\{x\} * \mathcal{F}\{y\}(f)$.

For ease of exposition we consider continuous time memoryless sampling, i.e., inter-sample times drawn from an exponential distribution with parameter λ . The spectral density of $A(t)$ is given, e.g., in [7] as $\Psi_A(f) = \lambda^2\delta(f) + \lambda$ with the well known Dirac delta function $\delta(f)$ that is defined as $\int_{-\infty}^{\infty} g(f)\delta(f)df = g(0)$ [14]. From (12) we calculate the spectral density of the observed process $W(t)$ as

$$\begin{aligned} \Psi_W(f) &= \Psi_A(f) * \Psi_Y(f) \\ &= (\lambda^2\delta(f) + \lambda) * \Psi_Y(f) \\ &= \lambda^2\Psi_Y(f) + \lambda(\sigma_Y^2 + \mu_Y^2) \end{aligned} \quad (13)$$

The convolution $\lambda * \Psi_Y(f)$ reduces to $\lambda(\sigma_Y^2 + \mu_Y^2)$ using the Wiener-Khinchin theorem as $\lambda \int_{-\infty}^{\infty} \Psi_Y(f)df = \lambda E[Y(t)^2]$. Consequently, the spectral density of $Y(t)$ can be estimated by solving (13) for $\Psi_Y(f)$. The estimate $\Psi_Y(f)$ requires estimates of the mean and variance of the traffic process, i.e., μ_Y and σ_Y^2 respectively, that can be obtained as in Sect. IV-A. An estimate of H is obtained from the slope of $\Psi_Y(f)$ on a log-log scale.

Next, we consider periodic sampling in conjunction with the spectral density method. For periodic sampling it is known that the sampling frequency has to be twice the highest frequency contained in the sampled process to avoid aliasing. This is known as Nyquist criterion. For periodic sampling $\Psi_A(f)$ is a dirac comb with inter-dirac distances of $1/\Delta$ where Δ is the sampling period. This leads to a repetition of the spectrum

$\Psi_Y(f)$ at distances $1/\Delta$. An *irreversible* spectral overlap occurs if the Nyquist criterion is not met, which is the case here as $\Psi_Y(f)$ is not band limited. As a result the method of spectral estimation of the Hurst parameter cannot be used directly with periodic sampling. Also, the remaining sampling strategies from Sect. III-A may not yield an expression for $\Psi_W(f)$ in (13) that can be solved for $\Psi_Y(f)$.

As in Sect. III we find that geometric sampling provides a substantial advantage when deploying established H estimators to sampled observations. For the considered methods, (11) and (13) provide the measures needed for H estimation.

V. ACTIVE PROBING

So far, we focused on the estimation of traffic correlations using passive sampling. In large multi-provider networks like the Internet, service providers often do not provide such network traces, e.g., for reasons of competition. The estimation of traffic correlations, therefore, must rely on inferring samples of the Internet traffic from network metrics that can be easily observed at end systems, e.g., by active probes. Moreover, passive sampling is a priori limited to single links. In case of network paths, where the correlations of the end-to-end service involve multiple nodes and links, end-to-end measurements may be the only viable option. We present an active probing method that enables users to characterize end-to-end paths, with minimal effort and without administrative support from the network under observation.

In this section, we address the fundamental problem of inferring the correlation of LRD traffic using active probes. We propose a new active probing method which collects traffic samples by detecting router busy periods. The observations are used to estimate the covariance of the end-to-end service. Subsequently, we estimate the corresponding Hurst parameter. Furthermore, we show that the well known packet pair dispersions approach, which captures the traffic intensity at the ingress of a router, is also applicable for the derivation of LRD traffic correlations. In the sequel, we describe our probing methodology and discuss traffic correlation estimation for both the single and multi-node cases. We then show testbed measurements to demonstrate the feasibility of our method. Finally, we present a set of Internet measurement results showing end-to-end correlations of entire network paths.

A. Probing methodology

We investigate two probing methods that facilitate the inference of certain characteristics of network traffic, referred to as cross traffic. The two methods differ with respect to the probes, i.e., single packets and packet pairs, and the observed metric, i.e., delay and packet pair dispersion, respectively.

1) *Single packet probes*: To extract an estimate of the cross traffic autocovariance, we propose an approach which uses the delays of single packet probes to detect busy periods at a router, and hence samples the link utilization at the router egress. For the remainder of this work, cross traffic denotes any traffic sharing resources with the probing traffic.

We make the general assumption that packet scheduling is non-preemptive. Hence, whenever a router is busy transmitting a packet, the delay d_p experienced by an arriving packet will be greater than the minimal delay d_{min} experienced when the router is idle. Consequently, we can sample cross traffic increments at the router egress, by injecting probe packets and analyzing their delays. For each probe, we measure the one way delay $d_p = t_r - t_s$, using the send and receive times t_s and t_r , respectively. To determine if the router was busy, we check whether the observed delay d_p is greater than the minimum network delay d_{min} . As a result, each probe yields a sample of the egress link state at time $t = t_s$, and the observed process can be constructed as

$$W(t) = \begin{cases} 1 & \text{if } d_p > d_{min} \text{ and } A(t) = 1 \\ 0 & \text{otherwise.} \end{cases} \quad (14)$$

It is known [11], [13], that the covariance structure of LRD traffic is preserved at the output of a queue or a traffic shaper, such that $W(t)$ permits observing the covariance of the cross traffic. We assume that the perturbation of the observed traffic due to probe size and probing rate is negligible, since the probing rates used are typically less than one per mill of the capacity. Furthermore, as we can assume that dropped probes are due to a busy router, we account for lost probing packets by setting $W(t) = 1$ for all dropped probes of $A(t)$.

2) *Packet pair probes*: In the following we present a second probing technique to estimate the cross traffic autocovariance that uses the dispersion of packet pair probes. Packet pair probing is a popular method for estimating the available bandwidth of a bottleneck link with FIFO queueing, e.g., [38]. A probe consists of two packets, each of size L , that are sent into the network back-to-back. The gap between the packet send times $t_{s,1}$ and $t_{s,2}$ is set to $g_s = t_{s,2} - t_{s,1} = L/C$, where C is the capacity of the bottleneck link. The subscript denotes the packet location and number, e.g., $t_{s,1}$ denotes the time stamp of the first packet of the probe pair at the sender. The packet pair dispersion $g_r = t_{r,2} - t_{r,1}$ observed at a receiver yields a sample of the cross traffic intensity $W(t)$ at $t = t_{s,1}$ as [38]

$$W(t) = C \left(\frac{g_r - g_s}{g_s} \right). \quad (15)$$

We set $W(t) = 0$ if no probe is sent at t as well as if probes are lost or incomplete at the receiver.

We apply this method to infer cross traffic intensities by injecting packet pair probes at times t_s and measuring the packet dispersion g_r at the probe receiver. Note that the multiplicative constant g_s/C in (15) does not alter the covariance structure. Hence, we can drop g_s/C and estimate the covariance of the cross traffic process from $W(t) = g_r - g_s$ if $A(t) = 1$ and zero otherwise without knowing the absolute value of the bottleneck link capacity.

The packet pair method requires a sufficiently accurate time stamp resolution at the receiver to correctly capture the variations in g_r . As the first packet functions as a time reference, while the traffic intensity is sampled by the second packet,

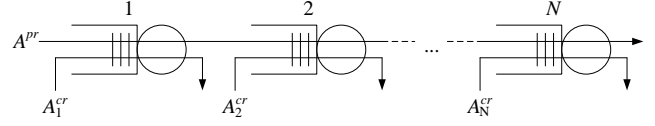


Fig. 6: N node topology with probing traffic A^{pr} and LRD cross traffic A_i^{cr} for nodes $i \in [1, N]$.

the approach does not require a synchronization between the sender and receiver clocks. However, this results in an overhead associated with each probe. As an example, when equally sized packets are used, 50% of the probing load is “wasted”, thereby reducing the effective sampling resolution for a given probing rate by a factor of two. In addition, the extension of packet pair probing to the multi-node case is not trivial. Therefore, we proceed using the first method, i.e., by detecting router busy periods.

B. Measuring LRD in single- and multi-node scenarios

In this subsection we consider estimating traffic correlations in multi-node scenarios using the busy period detection technique (14). We now show that the observed process $W_N(t)$ at the egress of an N node path with LRD cross traffic also exhibits LRD behavior. Moreover, for cross traffic characterized by different Hurst parameters, we show that the largest Hurst parameter dominates the covariance of the observed process $W_N(t)$. These results are in agreement with [13] which shows that the largest Hurst parameter dominates end-to-end performance.

Consider an N node topology with independent LRD cross traffic as in Fig. 6. We describe the busy state of each node using the processes $Y_i(t)$ for node $i \in [1, N]$. Hence, $Y_i(t) = 1$ if node i is busy at time t and $Y_i(t) = 0$ otherwise. Note that the covariance $c_{Y_i}(\tau) \sim \tau^{2H_i-2}$ measured at the egress of node i has the same LRD property as the cross traffic input at the node [11], [13]. Next, consider an active probe that is injected into the path. After subtracting the minimum end-to-end delay d_{min} the observer at the egress of the path will measure a positive delay only if any of the routers was busy when the probe arrived at the respective router. Otherwise, the probe delay will equal zero. Hence, $W_N(t)$ is the logical OR operation of the individual processes $Y_i(t)$ for $i \in [1, N]$. Since $Y_i(t)$ and $W_i(t) \in \{0, 1\}$, we straightforwardly find $W_i(t)$ at the egress of node i as

$$W_i(t) = \begin{cases} Y_1(t) & , i = 1 \\ W_{i-1}(t) + Y_i(t) - W_{i-1}(t)Y_i(t) & , i \in [2, N]. \end{cases} \quad (16)$$

For ease of exposition, (16) assumes that a node that is idle forwards probe packets instantaneously to the next node, such that the probe packet observes $Y_i(t)$ at the same time instance t for all $i \in [1, N]$. Dispensing with this assumption, (16) can be formulated in the same way requiring, however, additional notation as a probe packet observes $Y_i(t)$ at $t = t_i$ where $t_i \geq t_{i-1}$ for $i \in [2, N]$.

First, we illustrate (16) using a two node example and two independent LRD processes $Y_1(t)$, $Y_2(t)$. The observed

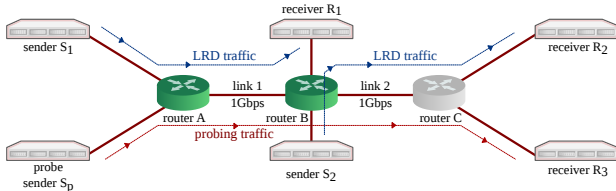


Fig. 7: Experimental setup: Emulab testbed

process at the egress of node 2 is $W_2(t) = 1$ if $Y_1(t) = 1$ OR $Y_2(t) = 1$ and $W_2(t) = 0$ otherwise, such that we deduce

$$W_2(t) = Y_1(t) + Y_2(t) - Y_1(t)Y_2(t).$$

We derive the observed covariance $c_{W_2}(\tau)$ of $W_2(t)$ after some algebra as

$$c_{W_2}(\tau) = c_{Y_1}(\tau)c_{Y_2}(\tau) + c_{Y_1}(\tau)(1 - \mu_{Y_2})^2 + c_{Y_2}(\tau)(1 - \mu_{Y_1})^2.$$

The equation above directly shows that for large τ the covariance $c_{W_2}(\tau)$ is dominated by $c_{Y_i}(\tau)$ with the largest Hurst parameter, i.e., slowest decay. The covariance of the N -node end-to-end observations $c_{W_N}(\tau)$ is obtained using the recursion formula (16) as

$$c_{W_i}(\tau) = c_{W_{i-1}}(\tau)c_{Y_i}(\tau) + c_{W_{i-1}}(\tau)(1 - \mu_{Y_i})^2 + c_{Y_i}(\tau)(1 - \mu_{W_{i-1}})^2. \quad (17)$$

Using recursive substitution, it can be shown that the covariance of the end-to-end observations $c_{W_N}(\tau)$ is dominated by $c_{Y_i}(\tau)$ with the largest Hurst parameter for $i \in [1, N]$.

C. Probing Software and Experimental Setup

We developed a probing tool *H-probe*, available at [5], that performs online measurements to infer the covariance structure of the round trip service of network paths. *H-probe* injects ICMP echo request probes from the sender to the receiver and captures the associated round trip times using *libpcap*. In contrast to the (optional) client/server delay measurements using UDP, the use of ICMP probes is significantly more practical, as it circumvents clock synchronization issues and enables probing the path to any network host without the need for a receiver software. *H-probe* uses the method described in Sect. V-A and the statistical analysis discussed in Sect. III-A and optionally the H estimation technique from Sect. IV-A. For H estimation using the aggregate variance method a range of scales has to be fixed for the estimation [4]. A similar observation is made in the context of Hurst parameter estimation using wavelet decomposition [43]. The authors in [43] describe upper and lower cutoff bounds on the time scales considered for the estimation using wavelets. Similarly, we fix the range of scales M for the H estimation with upper and lower cutoffs M^{up} resp. M^{low} . We define the upper range end M^{up} depending on the sample size T , i.e., $T/M^{up} = 10^2$ to ensure enough points for the variance calculation at $M = M^{up}$. We fix $M^{low} = 0.1$ s. This range is consistent with the ranges reported in trace driven H estimation literature, e.g., [15], [44].

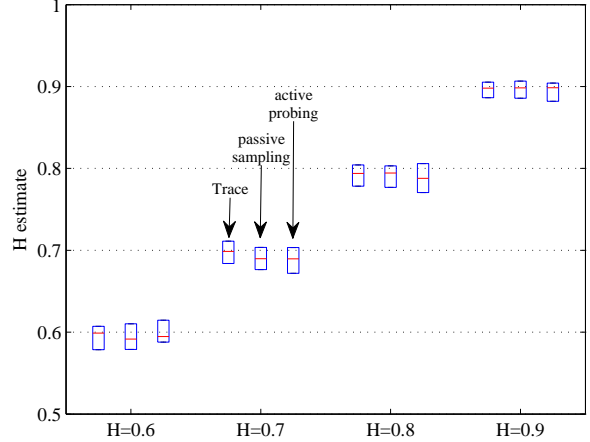


Fig. 8: Hurst parameter estimates from (a) offline trace analysis, (b) offline trace sampling and (c) active probing in the Emulab testbed.

In the following we present results obtained using this software package. Fig. 7 depicts the experimental setup in our Emulab-based testbed⁴. The topology comprises two relevant links, denoted link 1 and 2. Two traffic senders S_i , $i \in [1, 2]$ transmit LRD cross traffic traces with defined Hurst parameter H to the receivers R_i . The traces were synthesized by superposition of 10^5 heavy tailed on-off sources with tail index α . The relation between H and the tail index α is given in [45]. We set the mean rate of the traffic at *each* sender to 50 Mbps, with a constant packet size of 1500 Byte.

We use geometrically distributed inter-sample times with $p = 0.1$ and slot length $\delta = 1$ ms. For each measurement we send 10^6 probes with a mean probing rate of 100 packets per second (corresponding to ~ 70 kbps) from the probe sender S_p to the receiver R_3 . We use the same parameters for the Internet measurements, substituting R_3 with PlanetLab nodes. To deal with non-queueing induced jitter in routers, *H-probe* substitutes d_{min} in (14) by the average $E[d]$. This significantly reduces the measurement noise, because we can assume the distribution of this jitter is light tailed. We set the length of each measurement to 3 hours over which we assume stationarity of the traffic processes.

D. Testbed measurements

We deploy *H-probe* in our Emulab testbed, in order to verify its functionality in a controlled environment. First, we inject synthetic LRD traffic with $H \in [0.6, 0.9]$ on link 1 and collect 10^6 samples using our software. We repeat each experiment 25 times. We compare the covariance of the full traffic traces calculated offline (denoted trace) to the covariance extracted offline from a sampled process (denoted passive

⁴We use nodes with Supermicro X8DTU server mainboards with 2.2Ghz Intel E5520 Xeon processors, quad port Intel 82576EB Gigabit Ethernet Controllers, and Ubuntu 10.04 LTS with kernel 2.6.32-24, FIFO scheduling and buffers for 5000 packets. All links have a capacity of $C = 1$ Gbps.

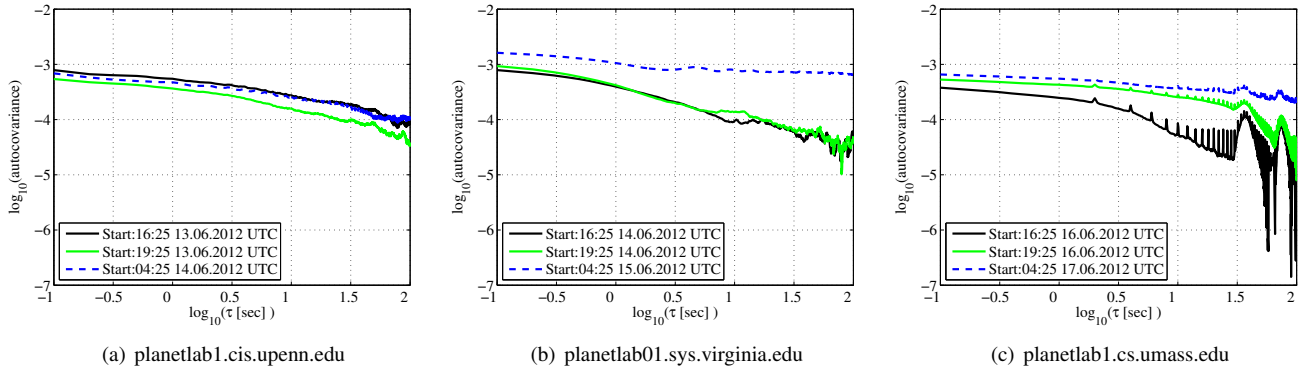


Fig. 9: End-to-end covariance estimates from Internet measurements. The covariance structure varies across different paths and for different times. For some targets we observe distinct periodicities on different time scales.

TABLE II: Mean Hurst parameter estimates using packet pair probes.

	configured H			
	0.6	0.7	0.8	0.9
estimated H	0.64	0.71	0.79	0.87

sampling) as well as from probes using H -probe (denoted active probing). To this end, we estimate the Hurst parameter using a least square regression of the estimated covariance on lags $\tau \in [10^0, 10^3]$. The lag range for the regression as well as the probing process parameters are chosen according to the constraints in Sect. III-B. We show boxplots of the corresponding Hurst parameters in Fig. 8. It is evident that H -probe correctly estimates the configured Hurst parameters.

We exemplarily deploy the packet pair dispersion method described in Sect. V-A2 in our Emulab testbed using the topology in Fig. 7. We measure the send and receive times of the probes using an Endace DAG packet capture card attached to network taps at the outgoing resp. incoming ports at S_p respectively R_3 . The recorded time stamps $t_s, t_r \in \mathbb{R}$ have a 7.5 ns capture precision. Tab. II includes the mean of estimated H over 25 runs. The results indicate that capturing cross traffic intensities using packet pairs can be successfully used for Hurst parameter estimation.

In another experiment we inject LRD traffic with differing H along links 1 and 2 denoted H_1 and H_2 respectively. In Tab. III we show exemplary Hurst parameters obtained for all combinations of $H_1 = \{0.6, 0.9\}$ and $H_2 = \{0.6, 0.9\}$ as obtained from single packet probes. We note that our method correctly characterizes the dominant correlations, respectively, H along end-to-end paths from a probing rate of as low as 70 kbps.

E. Internet measurements

We perform measurements over multiple weeks using H -probe from our lab in Germany targeting a number of worldwide PlanetLab nodes, in order to estimate the correlations on end-to-end paths across the Internet. The complex correlation

TABLE III: Exemplary Hurst parameter estimates in a 2 node scenario using single packet probes.

	estimated H on run #				
	1	2	3	4	5
$\{H_1 = 0.6, H_2 = 0.9\}$	0.87	0.89	0.89	0.90	0.90
$\{H_1 = 0.9, H_2 = 0.6\}$	0.87	0.88	0.88	0.90	0.90
$\{H_1 = 0.6, H_2 = 0.6\}$	0.59	0.62	0.64	0.63	0.63
$\{H_1 = 0.9, H_2 = 0.9\}$	0.92	0.92	0.89	0.92	0.89

structure along exemplary Internet paths is illustrated by the covariance plots in Fig. 9. First, we observe LRD covariance decay depicted in Fig. 9(a) and 9(b). We point out that the correlation and hence the Hurst parameter vary significantly throughout the day. Moreover, we find that the correlation structure varies strongly across different paths. Additionally, for some targets we observed distinct periodicities on different timescales, as exemplified in Fig. 9(c). Periodic behavior in offline Internet traces due to various protocol implementations has been previously reported, e.g., in [6]. Fig. 10 depicts estimated H using the aggregate variance method from Sect. IV-A. The Hurst parameter estimates indicate a diurnal behavior. We provide additional data sets and results in the appendix VIII.

H -probe provides a new tool enabling researchers to shed light on the complex structure of traffic correlations without requiring the availability of traffic traces from Internet service providers.

VI. CONCLUSIONS

In this paper, we derived estimators for the correlations of network traffic, given a limited set of traffic samples obtained by passive monitoring or active probing. We explored the impact of different sampling strategies on observed traffic correlations and quantified the impact of sampling on the observations. We showed that for finite sample sizes there are intrinsic limitations on the accuracy of the estimates and showed the influence of different sampling parameters. We

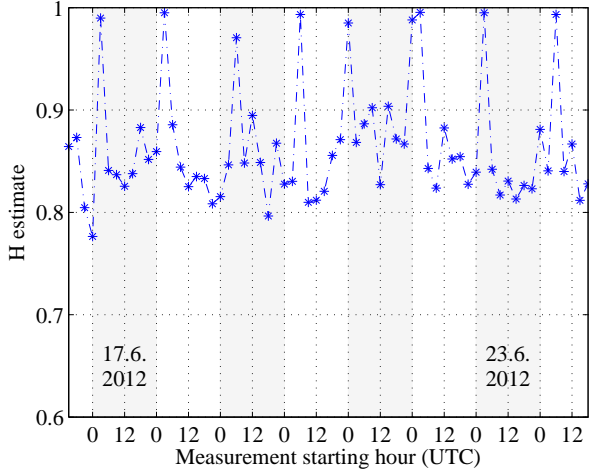


Fig. 10: Hurst parameter estimates from continues measurements over one week. Target is planetlab1.cis.upenn.edu. H estimates obtained from the aggregate variance method.

found a non-linear tradeoff between sampling duration and sampling intensity. Further, we inferred the Hurst parameter H from covariance estimates to quantify LRD. We developed and deployed an active probing method that estimates traffic correlations from end-to-end measurements without network support. The corresponding software is made publicly available. Finally, we presented measurement results from a controlled testbed environment as well as Internet paths. We observe a complex correlation structure on Internet paths. The correlation structure as well as H significantly vary across time and paths. In addition to LRD we observe periodic behavior at different time scales.

VII. APPENDIX

A. Autocorrelation of sampling point processes:

We rephrase a basic result from [7] that is essential for the following derivations. Given a stationary stochastic process $A(\tau)$ in continuous time τ that takes values of either zero or one (Kronecker delta). The times between two Kronecker deltas are independent and identically distributed according to a density function $f(\tau)$. The autocorrelation density of $A(\tau)$ is known for lags $\tau > 0$ as [7] Eq. (4.6.1)

$$E[A(t)A(t+\tau)] = \mu_A \sum_{n=1}^{\infty} f^{(*n)}(\tau) \quad (18)$$

where $f^{(*n)}(\tau)$ is the n -fold self-convolution of $f(\tau)$. The intuition behind (18) is that starting from one Kronecker delta at $A(t)$, another Kronecker delta at $A(t+\tau)$ can be the first, the second, the third ..., delta to come after the one at $A(t)$. The derivation in [7] uses a small time interval of length $\Delta t \rightarrow 0$, such that $\mu_A \Delta t$ is the probability that a Kronecker delta occurred in $[t, t+\Delta t)$ Eq. (4.5.9). To calculate the correlations of $A(t)$ [7] deduces the conditional probability that a Kronecker delta occurred at $[t+\tau, t+\tau+\Delta t)$ given a Kronecker delta at $[t, t+\Delta t)$. This is given by $\sum_{n=1}^{\infty} f^{(*n)}(\tau) \Delta t$ Eq. (4.5.11).

It follows that $(\Delta t)^2 \mu_A \sum_{n=1}^{\infty} f^{(*n)}(\tau)$ is the correlation of Kronecker deltas observed in time slots of length Δt .

A discrete-time extension of the correlation calculation from [7] with probability mass functions is straightforward. To this end we replace the probability density functions by probability mass functions and consider a time slot $\Delta t = 1$ such that we obtain correlation functions instead of densities.

For the continuous time distributions considered in this work we regard the correlations on fixed time slot basis. We use a discretization with a time slot of unit size.

B. Geometric sampling:

Given a discrete time sampling process $A(\tau)$ with inter-sample times drawn from a geometric distribution given in Tab. I with parameter p . The n -fold self-convolution of $f(\tau)$ is the probability mass function (pmf) of the sum of n geometrically distributed random variables, i.e., negative binomial distributed with parameters p and n [14]. We insert the pmf from [14] for $f^{(*n)}(\tau)$ into (18) to find

$$\begin{aligned} E[A(t)A(t+\tau)] &= \mu_A \sum_{n=1}^{\infty} \binom{\tau-1}{n-1} p^n (1-p)^{\tau-n} \\ &= \mu_A \sum_{n=1}^{\tau} \binom{\tau-1}{n-1} p^n (1-p)^{\tau-n} \\ &= \mu_A \sum_{s=0}^{\tau-1} \binom{\tau-1}{s} p^s (1-p)^{\tau-1-s} \\ &= \mu_A p^{\tau-1} \\ &= \mu_A^2. \end{aligned}$$

In the second line we used the support of the pmf $f^{(*n)}(\tau)$ to bound $1 \leq n \leq \tau$. In the third line we substituted $\tau-1 = l$ and $n-1 = s$. In the fourth line we used the binomial identity $\sum_{s=0}^l \binom{l}{s} x^s y^{l-s} = (x+y)^l$. Finally, we know from the geometric distribution that $\mu_A = p$.

C. Gamma sampling:

Given the time between two Kronecker deltas is Gamma distributed as in Tab. I with parameters α, β . The sum in (18) leads to the following expression

$$\sum_{n=1}^{\infty} f^{(*n)}(\tau) = \frac{e^{-\beta\tau}}{\tau} \sum_{n=1}^{\infty} \frac{(\beta\tau)^{n\alpha}}{\Gamma(n\alpha)}. \quad (19)$$

We derive analytical expressions for the cases $\alpha = 2$ and $\alpha = 4$ corresponding to Erlang(2) and Erlang(4) distributions of the inter-sample times. The mean rate of the sampling process is $\mu_A = \beta/\alpha$. We substitute $\alpha = 2$ into (19) and evaluate the sum in (19) as

$$\sum_{n=1}^{\infty} \frac{(\beta\tau)^{2n}}{(2n-1)!} = \beta\tau \sinh(\beta\tau)$$

using the series expansion for sinh from [1] Eq. (4.5.62). We then exploit the identity $\sinh(x) = (e^x - e^{-x})/2$ and that $\mu_A = \beta/2$ to evaluate (18) as

$$E[A(t)A(t+\tau)] = \mu_A^2 (1 - e^{-2\beta\tau})$$

For $\alpha = 4$ we evaluate the sum in (19) as

$$\sum_{n=1}^{\infty} \frac{(\beta\tau)^{4n}}{(4n-1)!} = \beta\tau \left(\frac{\sinh(\beta\tau) - \sin(\beta\tau)}{2} \right)$$

using the series expansion for \sinh and \sin from [1] Eq. (4.5.62) resp. Eq. (4.3.65). We insert this result into (18) to find

$$\mathbb{E}[A(t)A(t+\tau)] = \mu_A^2(1 - e^{-2\beta\tau} - 2\sin(\beta\tau)e^{-\beta\tau}).$$

using the identity $\sinh(x) = (e^x - e^{-x})/2$ and that $\mu_A = \beta/4$.

D. Uniform sampling:

Given the time between two Kronecker deltas is uniformly distributed with $f(\tau) = 1/b$ for $\tau \in [0, b]$ and zero otherwise. The mean rate of the sampling process is $\mu_A = 2/b$. In the following, we calculate the sum from (18) for $\tau \in [0, b]$. We expand $\sum_{n=1}^{\infty} f^{(*n)}(\tau)$ in (18) as

$$\begin{aligned} \sum_{n=1}^{\infty} f^{(*n)}(\tau) &= f(\tau) + \int_0^\tau f(x_1)f(\tau-x_1)dx_1 \\ &+ \int_0^\tau \int_0^{x_1} f(\tau-x_1)f(x_1-x_2)f(x_2)dx_1dx_2 \\ &+ \int_0^\tau \int_0^{x_1} \int_0^{x_2} f(\tau-x_1)f(x_1-x_2)f(x_2-x_3)f(x_3)dx_1dx_2dx_3 \\ &+ \dots \end{aligned} \quad (20)$$

Since all arguments (\cdot) of the pdf f in (20) are in the range $[0, \tau]$ we can replace all pdfs $f(\cdot)$ in (20) by $1/b$. Equation (20) evaluates then to the series expansion of the exponential function, i.e.,

$$\begin{aligned} \sum_{n=1}^{\infty} f^{(*n)}(\tau) &= \frac{1}{b} + \frac{\tau}{b^2} + \frac{\tau^2}{2!b^3} + \frac{\tau^3}{3!b^4} + \dots \\ &= \frac{1}{b} \sum_{n=0}^{\infty} \frac{(\tau/b)^n}{n!} \\ &= \frac{1}{b} e^{\tau/b} \end{aligned} \quad (21)$$

Finally, we use (21), (18), and that $\mu_A = 2/b$ to derive

$$\mathbb{E}[A(t)A(t+\tau)] = \frac{1}{2}\mu_A^2 e^{\tau/b}$$

for $\tau \in [0, b]$. Since the process is mixing [3], we conclude for $\tau > b$ that the autocorrelation $\mathbb{E}[A(t)A(t+\tau)]$ converges quickly to μ_A^2 .

E. Distribution of the autocovariance of geometrically sampled iid Gaussian sequences:

Given a sample path $w(t)$ of $W(t)$, that is described by (4), where $A(t)$ is a Bernoulli process and $Y(t)$ is a Gaussian iid process with mean μ_Y and variance σ_Y^2 . The mean of the observations is known as $\mu_W = \mu_A\mu_Y$. The variance of $W(t)$ is given by $\sigma_W^2 = \sigma_A^2\mu_Y^2 + \sigma_Y^2\mu_A^2 + \sigma_A^2\sigma_Y^2$ through independence of $A(t)$ and $Y(t)$. From the Bernoulli process $A(t)$ we know $\sigma_A^2 + \mu_A^2 = \mu_A$ such that we can write $\sigma_W^2 = \sigma_A^2\mu_Y^2 + \sigma_Y^2\mu_A$. We consider a limited sample size

T such that $w(t)$ given for $t \in [1, T]$. An unbiased estimator of the autocovariance $\tilde{c}_W(\tau)$ is

$$\tilde{c}_W(\tau) = \frac{1}{T-\tau} \sum_{t=1}^{T-\tau} (w(t) - \mu_W)(w(t+\tau) - \mu_W).$$

After expansion of the product, for large $T - \tau$ we apply the central limit theorem to approximate the individual terms by normal random variables to find

$$\begin{aligned} \tilde{c}_W(\tau) &\approx \mathcal{N}\left(\mu_W^2, \frac{\sigma_W^4 + 2\mu_W^2\sigma_W^2}{T-\tau}\right) - \mathcal{N}\left(2\mu_W^2, \frac{2\mu_W^2\sigma_W^2}{T-\tau}\right) + \mu_W^2 \\ &= \mathcal{N}\left(0, \frac{\sigma_W^4 + 4\mu_W^2\sigma_W^2}{T-\tau}\right). \end{aligned}$$

The confidence interval is directly obtained as 2 times the standard deviation, i.e., $\pm 2\sqrt{\sigma_W^4 + 4\mu_W^2\sigma_W^2}/\sqrt{(T-\tau)}$. Finally, we insert $\sigma_W^2 = \sigma_A^2\mu_Y^2 + \sigma_Y^2\mu_A$ and assume $T \gg \tau$ to find the confidence interval $\pm 2\sqrt{(\sigma_A^2\mu_Y^2 + \sigma_Y^2\mu_A)^2 + 4\mu_A^2\mu_Y^2(\sigma_A^2\mu_Y^2 + \sigma_Y^2\mu_A)}/\sqrt{T}$.

F. Distribution of the autocovariance of the geometric sampling process:

Given a sample path $a(t)$ of a Bernoulli sampling process $A(t)$ with a limited sample size T such that $A(t)$ is given for $t \in [1, T]$. The Bernoulli sampling process has geometrically distributed inter-sample times as in Tab. I. Given the mean μ_A is known. An unbiased estimator of the autocovariance $\tilde{c}_A(\tau)$ is

$$\tilde{c}_A(\tau) = \frac{1}{T-\tau} \sum_{t=1}^{T-\tau} (a(t) - \mu_A)(a(t+\tau) - \mu_A).$$

After expansion of the product, for large $T - \tau$ we apply the central limit theorem to approximate the individual terms by normal random variables to find

$$\begin{aligned} \tilde{c}_A(\tau) &\approx \mathcal{N}\left(\mu_A^2, \frac{\sigma_A^4 + 2\mu_A^2\sigma_A^2}{T-\tau}\right) - \mathcal{N}\left(2\mu_A^2, \frac{2\mu_A^2\sigma_A^2}{T-\tau}\right) + \mu_A^2 \\ &= \mathcal{N}\left(0, \frac{\sigma_A^4 + 4\mu_A^2\sigma_A^2}{T-\tau}\right). \end{aligned}$$

The confidence interval is directly obtained as 2 times the standard deviation, i.e., $\pm 2\sigma_A\sqrt{\sigma_A^2 + 4\mu_A^2}/\sqrt{T-\tau}$.

G. Bias of the autocovariance estimator for $Y(t)$:

We derive the bias of the covariance estimator (22) if applied to a sample path $y(t)$ of the LRD process $Y(t)$ and show that it is asymptotically unbiased as the sample duration tends to infinity $T \rightarrow \infty$. Given a sample path $y(t)$ with sample mean $\tilde{\mu}_{Y_0} = \frac{1}{(T-\tau)} \sum_{t=1}^{T-\tau} y(t)$ and $\tilde{\mu}_{Y_\tau} = \frac{1}{(T-\tau)} \sum_{t=1}^{T-\tau} y(t+\tau)$ a covariance estimator is

$$\tilde{c}_Y(\tau) = \frac{1}{T-\tau} \sum_{t=1}^{T-\tau} (y(t) - \tilde{\mu}_{Y_0})(y(t+\tau) - \tilde{\mu}_{Y_\tau}) \quad (22)$$

To estimate the bias, we derive the expected value $\mathbb{E}[\tilde{c}_Y(\tau)]$. To this end, we expand the product and compute the expected values of the individual terms $y(t)y(t+\tau) - y(t)\tilde{\mu}_{Y_\tau} - y(t+\tau)\tilde{\mu}_{Y_0} + \tilde{\mu}_{Y_0}\tilde{\mu}_{Y_\tau}$ as

$$\mathbb{E}\left[\frac{1}{T-\tau} \sum_{t=1}^{T-\tau} y(t)y(t+\tau)\right] = c_Y(\tau) + \mu_Y^2,$$

where $c_Y(\tau)$ and μ_Y are the population parameters, and

$$\mathbb{E} \left[\frac{1}{T-\tau} \sum_{t=1}^{T-\tau} y(t) \tilde{\mu}_{Y_\tau} \right] = \mathbb{E}[\tilde{\mu}_{Y_0} \tilde{\mu}_{Y_\tau}],$$

where we used that $\frac{1}{T-\tau} \sum_{t=1}^{T-\tau} y(t) = \tilde{\mu}_{Y_0}$. The same argument applies for the product $y(t+\tau) \tilde{\mu}_{Y_0}$. We estimate

$$\begin{aligned} \mathbb{E}[\tilde{\mu}_{Y_0} \tilde{\mu}_{Y_\tau}] &= \text{Cov}[\tilde{\mu}_{Y_0}, \tilde{\mu}_{Y_\tau}] + \mathbb{E}[\tilde{\mu}_{Y_0}] \mathbb{E}[\tilde{\mu}_{Y_\tau}] \\ &\leq \text{Var}[\tilde{\mu}_{Y_0}] + \mu_Y^2, \end{aligned}$$

with $\mathbb{E}[\tilde{\mu}_{Y_0}] = \mu_Y$, respectively, $\mathbb{E}[\tilde{\mu}_{Y_\tau}] = \mu_Y$ that are unbiased estimators of the population mean. Note that the samples that form $\tilde{\mu}_{Y_0}$ and $\tilde{\mu}_{Y_\tau}$ overlap by $T-2\tau$, such that for $\tau \ll T$ we have $\text{Cov}[\tilde{\mu}_{Y_0}, \tilde{\mu}_{Y_\tau}] \approx \text{Var}[\tilde{\mu}_{Y_0}]$. Finally, we use that the variance of the mean of $T-\tau$ samples of an LRD process decays as $\sigma_Y^2/(T-\tau)^{2-2H}$ to derive

$$\mathbb{E}[\tilde{\mu}_{Y_0} \tilde{\mu}_{Y_\tau}] \approx \frac{\sigma_Y^2}{(T-\tau)^{2-2H}} + \mu_Y^2.$$

Putting all pieces together we obtain

$$\begin{aligned} \mathbb{E}[\tilde{c}_Y(\tau)] &= c_Y(\tau) - \text{Cov}[\tilde{\mu}_{Y_0}, \tilde{\mu}_{Y_\tau}] \\ &\approx c_Y(\tau) - \frac{\sigma_Y^2}{(T-\tau)^{2-2H}}, \end{aligned} \quad (23)$$

i.e., the estimator underestimates the covariance, where the bias diminishes if $T-\tau$ is large. We note, that the bias cannot be easily eliminated if the prefactor $1/(T-\tau-1)$ is used instead of $1/(T-\tau)$ in (22), as it is typically done if the covariance is estimated using the sample mean.

H. Bias of the autocovariance estimator for $W(t)$:

We derive the bias of the covariance estimator (22) if applied to the observed process $W(t)$. We show that the estimator is asymptotically unbiased for large sample durations $T \rightarrow \infty$. Given a sample path $w(t)$ with sample mean $\tilde{\mu}_{W_0}$, respectively, $\tilde{\mu}_{W_\tau}$ defined in Sect. VII-G. We use the covariance estimator from (22). To estimate the bias we derive $\mathbb{E}[\tilde{c}_W(\tau)]$ from (23) as

$$\mathbb{E}[\tilde{c}_W(\tau)] = c_W(\tau) - \text{Cov}[\tilde{\mu}_{W_0}, \tilde{\mu}_{W_\tau}],$$

where $c_W(\tau)$ is the population parameter. As before we estimate $\text{Cov}[\tilde{\mu}_{W_0}, \tilde{\mu}_{W_\tau}] \approx \text{Var}[\tilde{\mu}_{W_0}]$ and express $\tilde{\mu}_{W_0}$ as a sum to compute the variance $\text{Var}[\tilde{\mu}_{W_0}]$ as

$$\text{Var}[\tilde{\mu}_{W_0}] = \frac{1}{(T-\tau)^2} \sum_{i=1}^{T-\tau} \sum_{j=1}^{T-\tau} \text{Cov}[w(i), w(j)],$$

where we use the identity

$$\text{Var} \left[\sum_{i=1}^n X_i \right] = \sum_{i=1}^n \sum_{j=1}^n \text{Cov}[X_i, X_j] \quad (24)$$

for random variables X_i , $i \in [1, n]$. Rearranging the statement above yields

$$\text{Var}[\tilde{\mu}_{W_0}] = \frac{c_W(0)}{T-\tau} + \frac{2}{(T-\tau)^2} \sum_{t=1}^{T-\tau-1} (T-\tau-t)c_W(t),$$

where we used the notation $\text{Cov}[w(t), w(t+\tau)] = c_W(\tau)$. The expected value of the sample covariance follows as

$$\begin{aligned} \mathbb{E}[\tilde{c}_W(\tau)] &\approx c_W(\tau) - \frac{c_W(0)}{T-\tau} \\ &\quad - \frac{2}{(T-\tau)^2} \sum_{t=1}^{T-\tau-1} (T-\tau-t)c_W(t). \end{aligned} \quad (25)$$

I. Aggregate variance of a sampled process:

Proof of Lem. 2: The aggregated version of the process $W(t)$ on the aggregation level M is defined for $k \in \mathbb{N}$ as

$$W^{(M)}(k) = \frac{1}{M} \sum_{t=1+(k-1)M}^{kM} W(t),$$

where M is the block size that is used for averaging. The variance of $W^{(M)}$ is obtained using the identity (24) as

$$\text{Var}(W^{(M)}) = \frac{1}{M^2} \sum_{i=1}^M \sum_{j=1}^M \text{Cov}(W(i), W(j)).$$

Using the notation $c_W(\tau) = \text{Cov}(W(i), W(i+\tau))$ we rearrange the previous statement as

$$\text{Var}(W^{(M)}) = \frac{c_W(0)}{M} + \frac{2}{M^2} \sum_{\tau=1}^{M-1} (M-\tau)c_W(\tau). \quad (26)$$

The same expression can be formulated for $\text{Var}(A^{(M)})$ and $\text{Var}(Y^{(M)})$ by substituting $c_A(\tau)$ resp. $c_Y(\tau)$ for $c_W(\tau)$ in (26). Next, we insert $c_W(\tau)$ from Lem. 1 into (26) to relate $\text{Var}(W^{(M)})$ to $\text{Var}(A^{(M)})$, $\text{Var}(Y^{(M)})$, $c_A(\tau)$ and $c_Y(\tau)$. We obtain

$$\begin{aligned} \text{Var}(W^{(M)}) &= \frac{1}{M} c_Y(0)(c_A(0) + \mu_A^2) + \frac{1}{M} c_A(0) \mu_Y^2 \\ &\quad + \frac{2}{M^2} \sum_{\tau=1}^{M-1} (M-\tau)(c_Y(\tau)(c_A(\tau) + \mu_A^2) + c_A(\tau) \mu_Y^2). \end{aligned}$$

After some reordering we arrive at

$$\begin{aligned} \text{Var}(W^{(M)}) &= \mu_Y^2 \frac{c_A(0)}{M} + \mu_Y^2 \frac{2}{M^2} \sum_{\tau=1}^{M-1} (M-\tau)c_A(\tau) \\ &\quad + \mu_A^2 \frac{c_Y(0)}{M} + \mu_A^2 \frac{2}{M^2} \sum_{\tau=1}^{M-1} (M-\tau)c_Y(\tau) \\ &\quad + \frac{1}{M} c_Y(0)c_A(0) + \frac{2}{M^2} \sum_{\tau=1}^{M-1} (M-\tau)c_Y(\tau)c_A(\tau) \end{aligned}$$

and by application of (26) we obtain

$$\begin{aligned} \text{Var}(W^{(M)}) &= \mu_Y^2 \text{Var}(A^{(M)}) + \mu_A^2 \text{Var}(Y^{(M)}) \\ &\quad + \frac{1}{M} c_Y(0)c_A(0) + \frac{2}{M^2} \sum_{\tau=1}^{M-1} (M-\tau)c_Y(\tau)c_A(\tau). \end{aligned}$$

■

VIII. DATA SETS FROM INTERNET MEASUREMENTS

We perform measurements over multiple weeks using *H-probe* from our lab in Germany targeting a number of worldwide PlanetLab nodes. Next, we describe the measurement setup:

- Discretization slot length $\delta = 1$ ms.
- Geometrically distributed inter-sample times with $p = 0.1$.
- Number of probes collected 10^6 (~ 3 hours)
- ICMP probing packets of size 64 Byte
- Probing rate 100 pkt/s ~ 70 kbps (24 Byte layer 2 overhead)

In the following we present a representative set of the measurement results, where the target is planetlab1.cis.upenn.edu. We show exemplary end-to-end covariance as well aggregate variance estimates at two different days. In addition, we show estimates of measurements starting at 10:45 UTC from 17-24.7.2012.

For the autocovariance as well as the aggregate variance method the slope of the curve is given by $2H - 2$. Slope estimates are obtained through least square regression. The H estimates from Internet measurements have a moderately higher variance compared to active probing results from Fig. 8. Further, the H estimates in Fig. 10 show diurnal behavior.

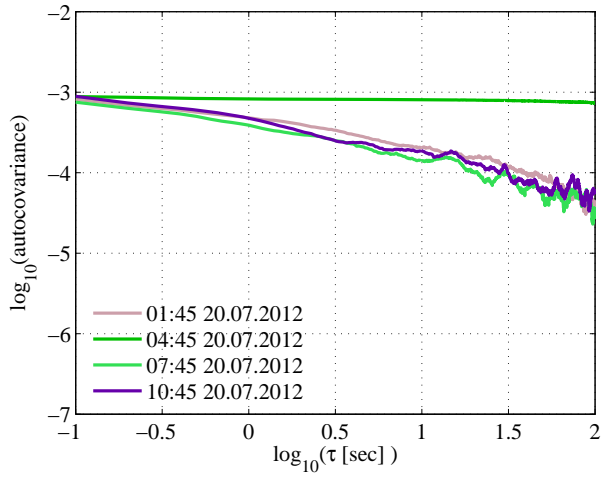


Fig. 11: Covariance estimates 20.7.2012 UTC

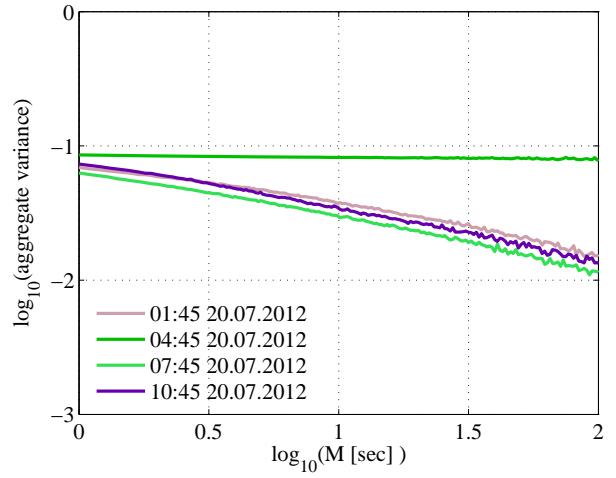


Fig. 14: Aggregate variance estimates 20.7.2012 UTC

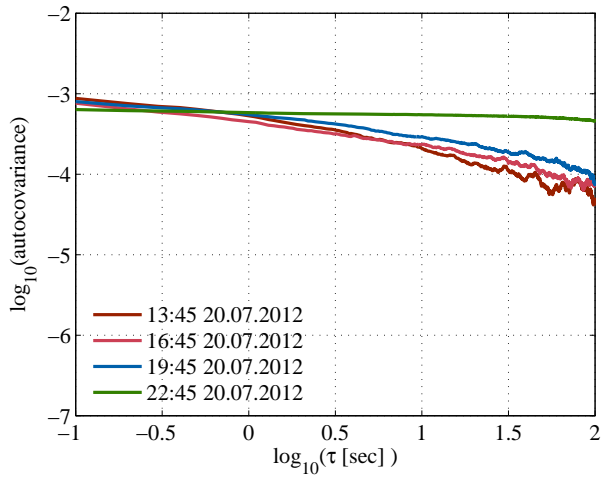


Fig. 12: Covariance estimates 20.7.2012 UTC

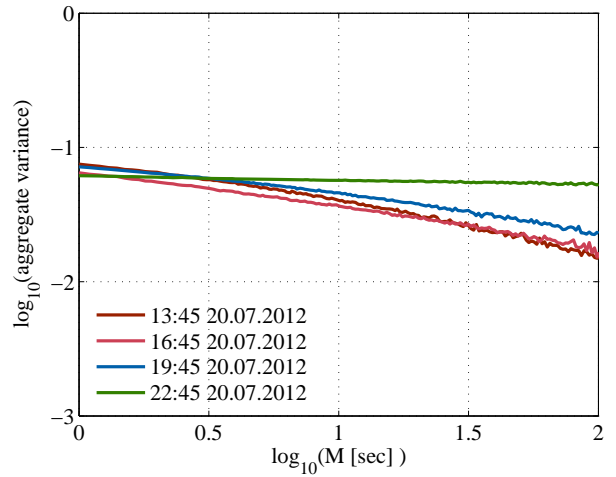


Fig. 15: Aggregate variance estimates 20.7.2012 UTC

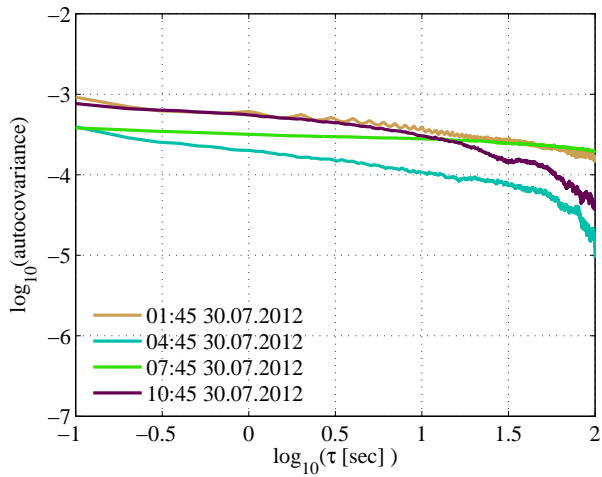


Fig. 13: Covariance estimates 30.7.2012 UTC

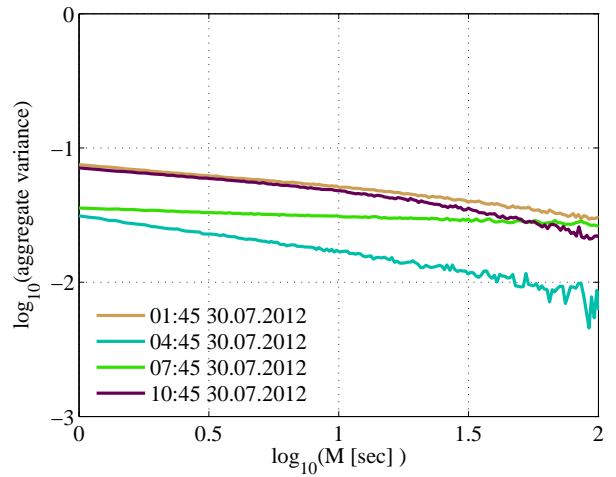


Fig. 16: Aggregate variance estimates 30.7.2012 UTC

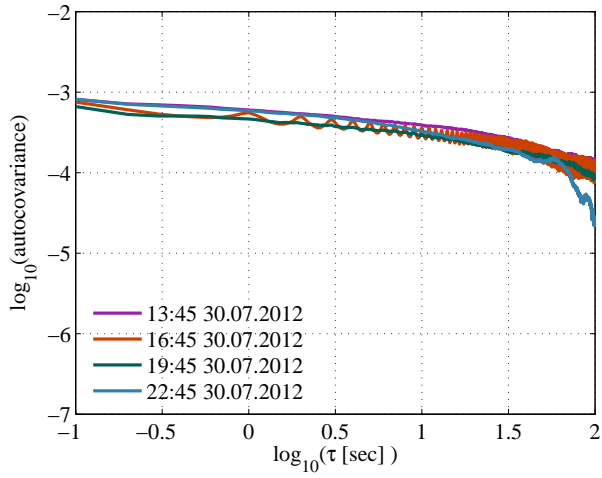


Fig. 17: Covariance estimates 30.7.2012 UTC

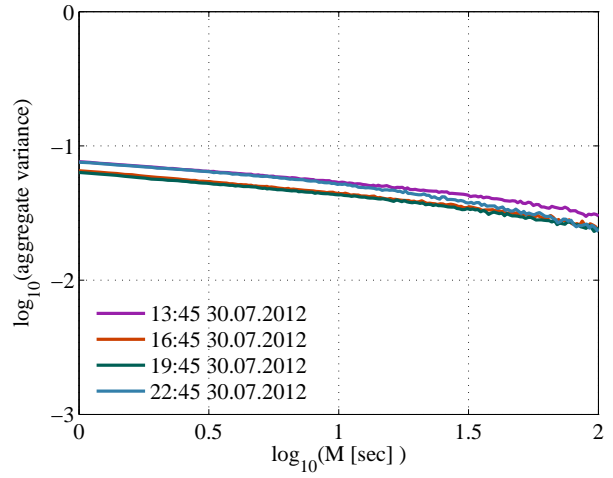


Fig. 20: Aggregate variance estimates 30.7.2012 UTC

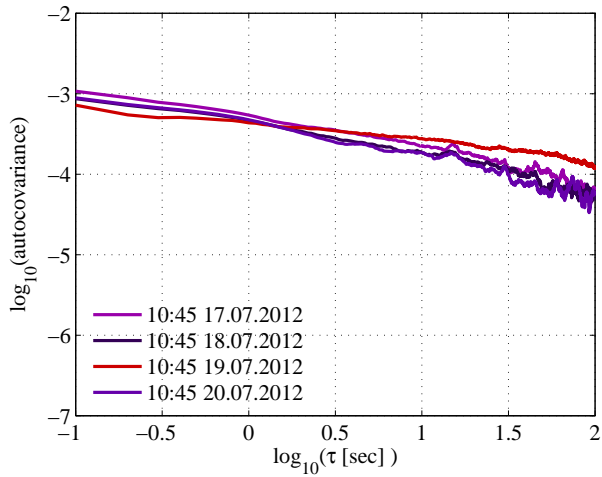


Fig. 18: Covariance estimates at 10:45 UTC

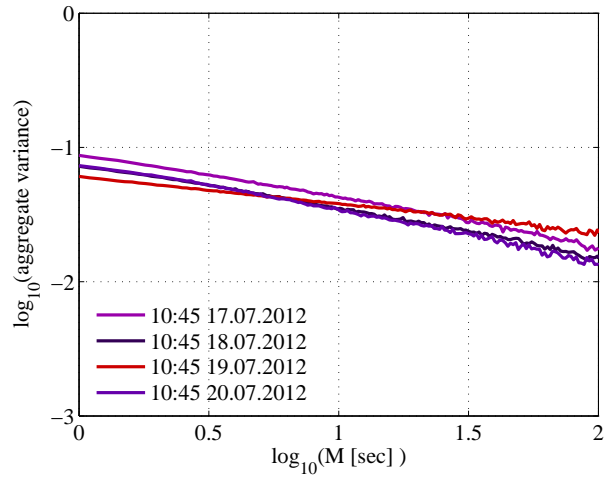


Fig. 21: Aggregate variance estimates at 10:45 UTC

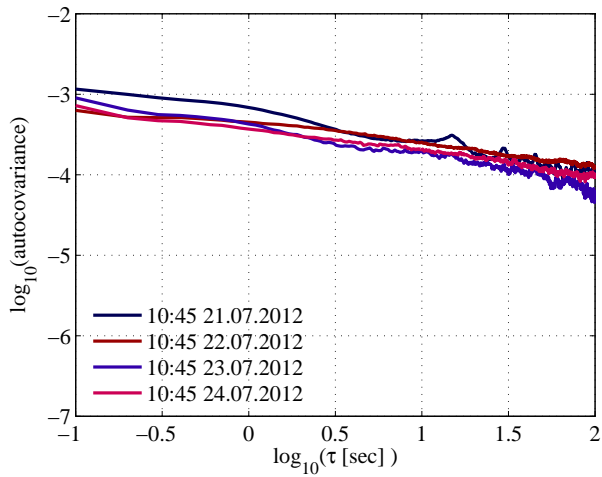


Fig. 19: Covariance estimates at 10:45 UTC

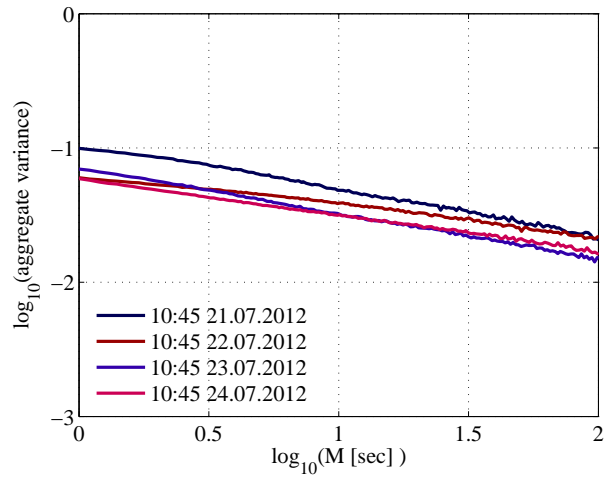


Fig. 22: Aggregate variance estimates at 10:45 UTC

REFERENCES

- [1] M. Abramowitz and I. Stegun. *Handbook of Mathematical Functions*. Dover, Dec. 1964.
- [2] F. Baccelli, S. Machiraju, D. Veitch, and J. Bolot. On optimal probing for delay and loss measurement. In *Proc. of IMC*, pages 291–302, 2007.
- [3] F. Baccelli, S. Machiraju, D. Veitch, and J. Bolot. The role of PASTA in network measurement. *IEEE/ACM Trans. Netw.*, 17(4):1340–1353, 2009.
- [4] J. Beran. *Statistics for Long-Memory Processes*. Chapman & Hall/CRC, Oct. 1994.
- [5] Z. Bozakov, A. Rizk, and M. Fidler. H-probe software, 2012. Available at: <http://www.ikt.uni-hannover.de/h-probe>.
- [6] A. Broido, R. King, E. Nemeth, and K. Claffy. Radon spectroscopy of inter-packet delay. In *Proc. of High Speed Networking Workshop*, 2003.
- [7] D. Cox and P. Lewis. *The statistical analysis of series of events*. Methuen's Statistical Monographs, 1966.
- [8] M. Crovella and A. Bestavros. Self-similarity in World Wide Web traffic: evidence and possible causes. *IEEE/ACM Trans. Netw.*, 5(6):835–846, Dec. 1997.
- [9] C. Dovrolis, P. Ramanathan, and D. Moore. What do packet dispersion techniques measure? In *Proc. of INFOCOM*, pages 905–914, 2001.
- [10] N. Duffield and N. O'Connell. Large deviations and overflow probabilities for the general single-server queue, with applications. *Math. Proc. Camb. Phil. Soc.*, 118(2):363–375, Sept. 1995.
- [11] A. Erramilli, O. Narayan, and W. Willinger. Experimental queueing analysis with long-range dependent packet traffic. *IEEE/ACM Trans. Netw.*, 4(2):209–223, 1996.
- [12] A. Feldmann, A. C. Gilbert, P. Huang, and W. Willinger. Dynamics of IP traffic: A study of the role of variability and the impact of control. In *Proc. of SIGCOMM*, pages 301–313, Aug. 1999.
- [13] A. Ganesh, N. O'Connell, and D. Wischik. *Big Queues*. Springer, 2004.
- [14] G. Grimmet and D. Stirzaker. *Probability and Random Processes*. Oxford University Press, 2001.
- [15] H. Gupta, A. Mahanti, and V. Ribeiro. Revisiting coexistence of poissonity and self-similarity in internet traffic. In *Proc. of MASCOTS*, pages 1–10, Sept. 2009.
- [16] G. He and J. Hou. On exploiting long range dependency of network traffic in measuring cross traffic on an end-to-end basis. In *Proc. of INFOCOM*, pages 1858–1868, 2003.
- [17] V. Jacobson. Pathchar: A tool to infer characteristics of internet paths, Apr. 1997.
- [18] M. Jain and C. Dovrolis. End-to-end available bandwidth: measurement methodology, dynamics, and relation with TCP throughput. *IEEE/ACM Trans. Netw.*, 11(4):537–549, Aug. 2003.
- [19] W. Leland, M. Taqqu, W. Willinger, and D. Wilson. On the self-similar nature of Ethernet traffic. *IEEE/ACM Trans. Netw.*, 2(1):1–15, Feb. 1994.
- [20] J. Liebeherr, A. Burchard, and F. Ciucu. Delay bounds in communication networks with heavy-tailed and self-similar traffic. *IEEE Trans. Inf. Theory*, 58(2):1010–1024, 2012.
- [21] X. Liu, K. Ravindran, and D. Loguinov. What signals do packet-pair dispersions carry? In *Proc. of INFOCOM*, pages 281–292, 2005.
- [22] X. Liu, K. Ravindran, and D. Loguinov. A queueing-theoretic foundation of available bandwidth estimation: Single-hop analysis. *IEEE/ACM Trans. Netw.*, 15(4):918–931, Aug. 2007.
- [23] P. Loiseau, P. Goncalves, G. Dewaele, P. Borgnat, P. Abry, and P. Primet. Investigating self-similarity and heavy-tailed distributions on a large-scale experimental facility. *IEEE/ACM Trans. Netw.*, 18(4):1261–1274, Aug. 2010.
- [24] S. Machiraju, D. Veitch, F. Baccelli, and J. Bolot. Adding definition to active probing. *Computer Communication Review*, 37(2):17–28, 2007.
- [25] M. Mandjes. *Large Deviations for Gaussian Queues*. Wiley & Sons, 2007.
- [26] L. Massouli and A. Simonian. Large buffer asymptotics for the queue with FBM input. *Applied Probability*, 36(3):894–906, Sept. 1999.
- [27] B. Melamed and W. Whitt. On arrivals that see time averages. *Oper. Res.*, 38(1):156–172, Feb. 1990.
- [28] I. Norros. On the use of fractional Brownian motion in the theory of connectionless networks. *IEEE J. Sel. Areas Commun.*, 13(6):953–962, Aug. 1995.
- [29] V. Paxson, G. Almes, J. Mahdavi, and M. Mathis. RFC2330 - Framework for IP Performance Metrics. <http://www.rfc-editor.org/rfc/rfc2330.txt>, 1998.
- [30] V. Paxson and S. Floyd. Wide-area traffic: The failure of Poisson modeling. *IEEE/ACM Trans. Netw.*, 3(3):226–244, 1995.
- [31] A. Philippe and M. Viano. Random sampling of long-memory stationary processes. *Journal of Statistical Planning and Inference*, 140(5):1110–1124, 2010.
- [32] V. Ribeiro, M. Coates, R. Riedi, S. Sarvotham, B. Hendricks, and R. Baraniuk. Multifractal cross-traffic estimation. In *Proc. of ITC Conference on IP Traffic, Modeling and Management*, Sep. 2000.
- [33] V. Ribeiro, R. H. Riedi, and R. Baraniuk. Optimal sampling strategies for multiscale stochastic processes. *IMS Lecture Notes - Monograph Series*, 49, Jan. 2006.
- [34] V. J. Ribeiro, R. H. Riedi, and R. Baraniuk. Multiscale queueing analysis. *IEEE/ACM Trans. Netw.*, 14(5):1005–1018, 2006.
- [35] A. Rizk and M. Fidler. Non-asymptotic end-to-end performance bounds for networks with long range dependent fbm cross traffic. *Computer Networks*, 56(1):127–141, 2012.
- [36] M. Roughan. Fundamental bounds on the accuracy of network performance measurements. In *Proc. of SIGMETRICS*, pages 253–264, 2005.
- [37] M. Roughan. A comparison of Poisson and uniform sampling for active measurements. *IEEE J. Sel. Areas Commun.*, 24(12):2299–2312, 2006.
- [38] J. Strauss, D. Katabi, and F. Kaashoek. A measurement study of available bandwidth estimation tools. In *Proc. of IMC*, pages 39–44, 2003.
- [39] M. Taqqu, V. Teverovsky, and W. Willinger. Estimators for long-range dependence: An empirical study. *Fractals*, 3(4):785–798, 1995.
- [40] M. Taqqu, W. Willinger, and R. Sherman. Proof of a fundamental result in self-similar traffic modeling. *Comput. Commun. Rev.*, 27(2):5–23, Apr. 1997.
- [41] M. B. Tariq, A. Dhamdhere, C. Dovrolis, and M. Ammar. Poisson versus periodic path probing (or, does PASTA matter). In *Proc. of IMC*, pages 119–124, 2005.
- [42] D. Veitch and P. Abry. A wavelet-based joint estimator of the parameters of long-range dependence. *IEEE Trans. Inf. Theory*, 45(2):878–897, Apr. 1999.
- [43] D. Veitch, P. Abry, and M. Taqqu. On the automatic selection of the onset of scaling. *Fractals*, 11(4):377–390, 2003.
- [44] D. Veitch, N. Hohn, and P. Abry. Multifractality in TCP/IP traffic: the case against. *Computer Networks*, 48:293–313, 2005.
- [45] W. Willinger, M. Taqqu, R. Sherman, and D. Wilson. Self-similarity through high-variability: statistical analysis of Ethernet LAN traffic at the source level. *IEEE/ACM Trans. Netw.*, 5(1):71–86, Feb. 1997.
- [46] R. Wolff. Poisson arrivals see time averages. *Operations Research*, 30(2):223–231, 1981.